AD-A146 518 AN INDIRECT MEASURE OF BELOW-GROUND ELECTRIC FIELD CONDUCTIVITY AND DIELECTRIC CONSTANT(U) HARRY DIAMOND LABS ADELPHI MD R P MANRIQUEZ ET AL. SEP 84 1/1

UNCLASSIFIED HDL-TR-2052 MIPR-HC1001-3-401 F/G 20/3 NL

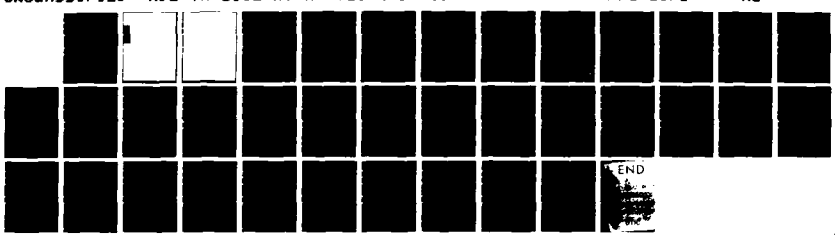

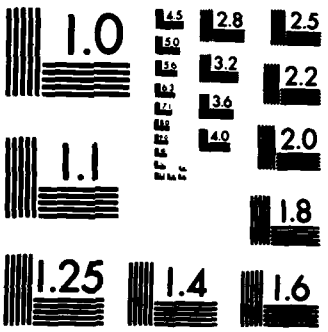

MICROCOPY RESOLUTION TEST CHART
NATIONAL BUREAU OF STANDARDS-1963-A

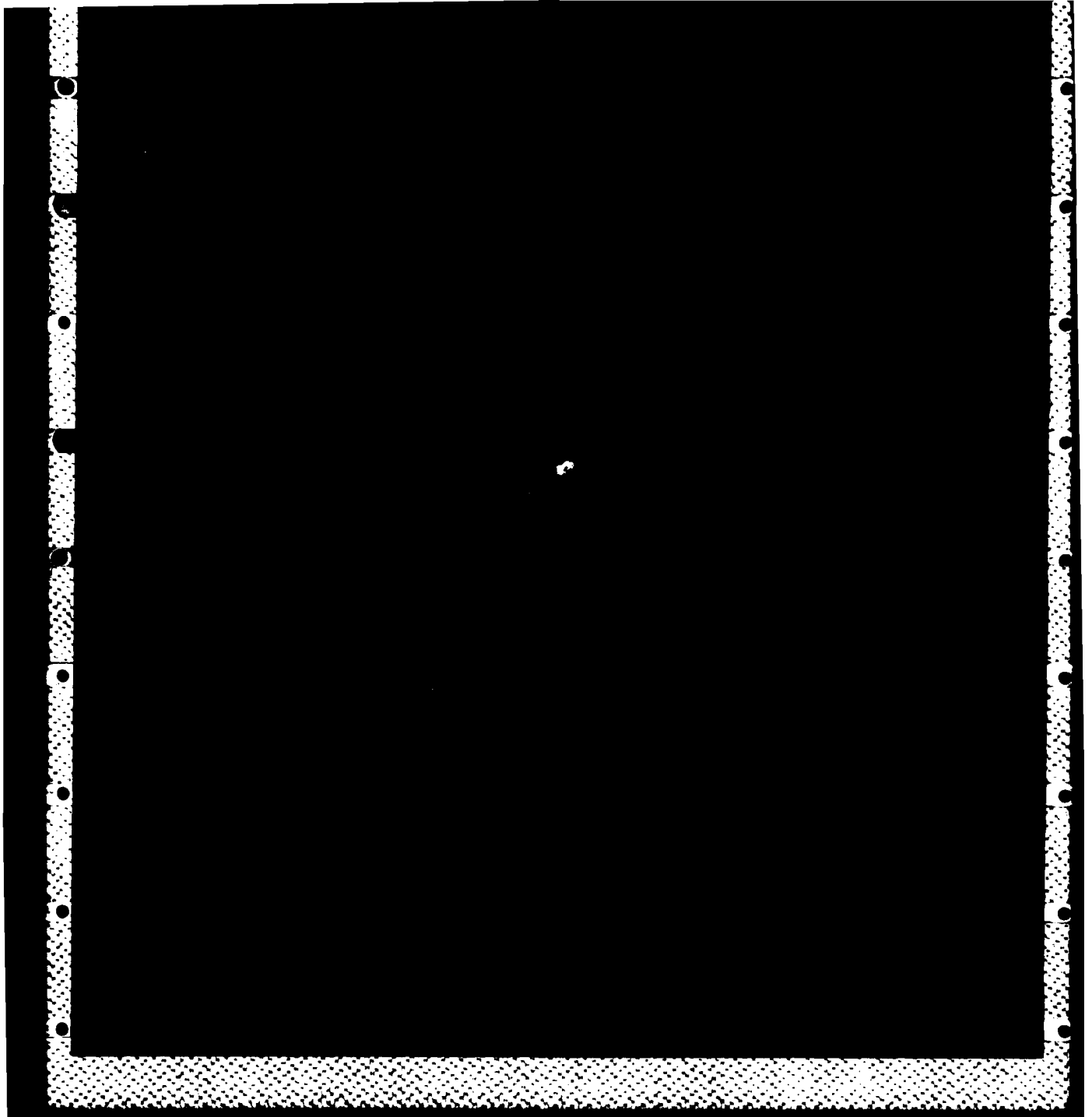

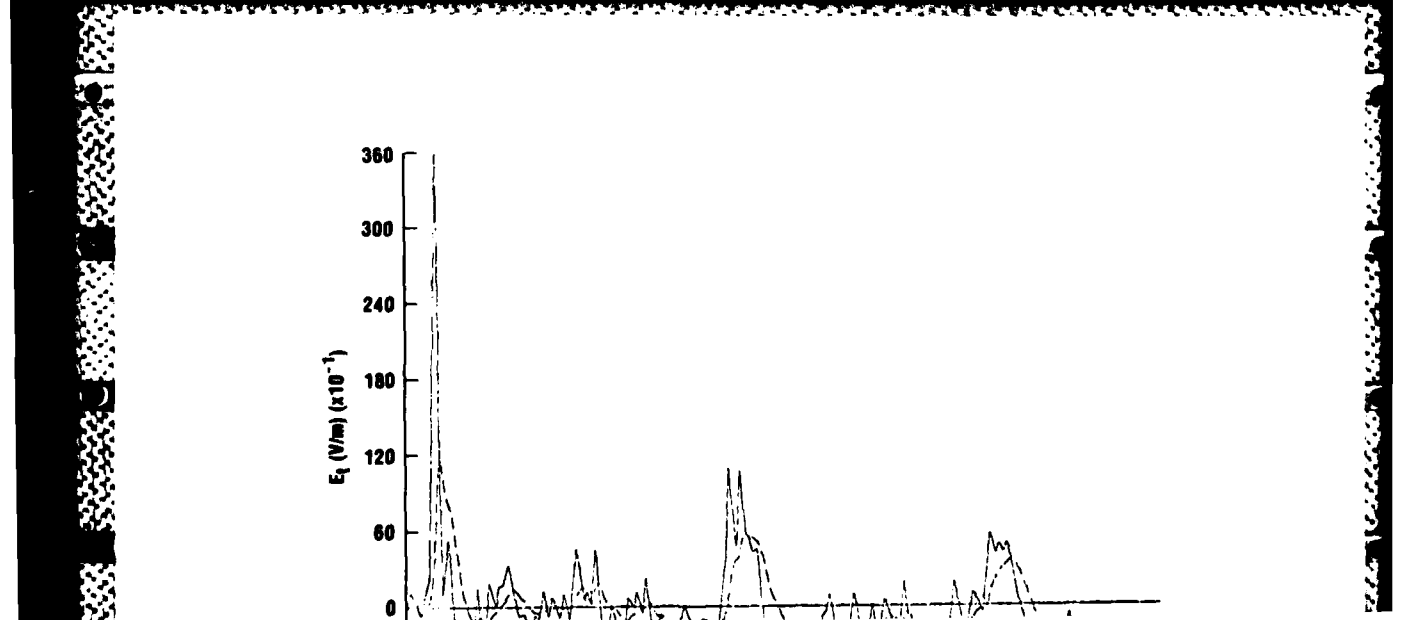
360
300
240
180
120
60
0
E_t (V/m) ($\times 10^{-1}$)

UNCLASSIFIED

SECURITY CLASSIFICATION OF THIS PAGE (When Data Entered)

REPORT DOCUMENTATION PAGE

READ INSTRUCTIONS BEFORE COMPLETING FORM

1. REPORT NUMBER HDL-TR-2052	2. GOVT ACCESSION NO. AD-A146 578
3. RECIPIENT'S CATALOG NUMBER	
4. TITLE (and Subtitle) An Indirect Measure of Below-Ground Electric Field, Conductivity, and Dielectric Constant	5. TYPE OF REPORT & PERIOD COVERED Technical Report
	6. PERFORMING ORG. REPORT NUMBER
7. AUTHOR(s) Rolando P. Manriquez John F. Sweton	8. CONTRACT OR GRANT NUMBER(s) PRON: WS3—8301WSA9 MIPR: HC1001-3-401
9. PERFORMING ORGANIZATION NAME AND ADDRESS Harry Diamond Laboratories 2800 Powder Mill Road Adelphi, MD 20783-1197	10. PROGRAM ELEMENT, PROJECT, TASK AREA & WORK UNIT NUMBERS Program Ele: 33126K
11. CONTROLLING OFFICE NAME AND ADDRESS National Communications System Office of the Manager Washington, DC 20305	12. REPORT DATE September 1984 13. NUMBER OF PAGES 38
14. MONITORING AGENCY NAME & ADDRESS(if different from Controlling Office)	15. SECURITY CLASS. (of this report) UNCLASSIFIED 15a. DECLASSIFICATION/DOWNGRADING SCHEDULE

16. DISTRIBUTION STATEMENT (of this Report)

Approved for public release; distribution unlimited.

17. DISTRIBUTION STATEMENT (of the abstract entered in Block 20, if different from Report)

18. SUPPLEMENTARY NOTES

HDL Project: E313E3
DRCMS Code: 33126K

19. KEY WORDS (Continue on reverse side if necessary and identify by block number)

EMP
Ground conductivity and dielectric constant
H field
Below-ground E field
REPS
Parallel-plate E-field sensor
Transfer function

20. ABSTRACT (Continue on reverse side if necessary and identify by block number)

This paper uses experimental data obtained on a buried, conducting, parallel-plate sensor to evaluate the electric field beneath the air/ground interface. The sensor is described with a simple equivalent circuit, and the characteristic response is evaluated both in time and frequency. The agreement between the calculated and measured transmitted electric field is quite good for reasonable values of constant and frequency-dependent electrical conductivity and dielectric permittivity of the ground. The electrical properties of the ground were the only parameters that needed to be adjusted to provide agreement between theory and experiment. Those values taken were considered within reasonable bounds.

DD FORM 1 JAN 73 1473 EDITION OF 1 NOV 65 IS OBSOLETE

UNCLASSIFIED

SECURITY CLASSIFICATION OF THIS PAGE (When Data Entered)

FOREWORD

The National Communications System (NCS) in response to Presidential Directive/NSC-53, "National Security Telecommunications Policy," is funding a comprehensive program on the effects of nuclear weapons on selected telecommunications systems. A portion of this effort is directed at determining the high-altitude electromagnetic pulse (EMP) vulnerability of the commercial Bell Telephone T1 Carrier systems, and at developing a T1 Carrier system specifically engineered to be EMP hard. The work described in this report was performed in support of these efforts.

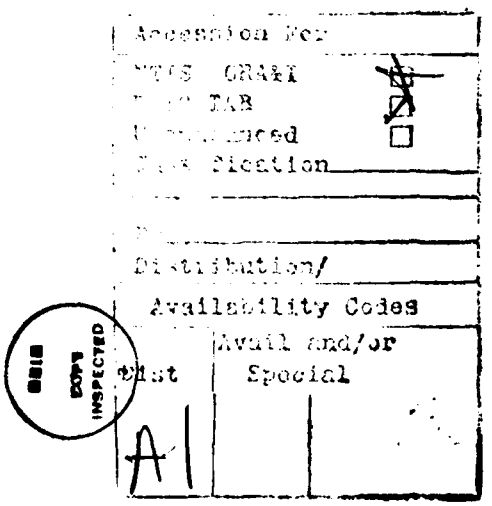

CONTENTS

FIGURES

FIGURES (Cont'd)

FIGURES (Cont'd)

1. INTRODUCTION

Analytical techniques exist for determining the electromagnetic (EMP) fields that are transmitted into the ground for given parameters of the ground and the incident field. The main objective of this paper is to indirectly measure the conductivity σ, dielectric constant ε_r, and electric (E) field below ground due to an incident EMP field as produced by the repetitive EMP simulator (REPS). REPS is a horizontal dipole radiator driven by a 1-MV repetitive pulse generator. The measurements were taken at the Harry Diamond Laboratories (HDL), Woodbridge Research Facility (WRF), Woodbridge, VA.

There are two methods to accomplish this objective:

(1) The determination of the "calculated" transmitted E field, E_t, from the measured magnetic field, H_x, at 1 m above ground, and the associated Maxwell equations and Fresnel coefficients in a continuous air/ground interface. The ground can be treated as a good conductor whose most important electrical parameters are conductivity and dielectric permittivity, ε.

(2) The determination of the "measured" transmitted E field from the induced voltage, V, across a buried capacitive parallel-plate E-field sensor with a plate separation ℓ. This V is "unfolded" from the measured voltage, V_o, at the sensor load through the use of the time-domain and frequency-domain solution techniques. The time-domain solution is derived from an equivalent circuit model of the E-field sensor. From this solution, the sensor can be characterized as an E-field sensor and an $\dot{E}$ (first derivative of E) field sensor. The frequency-domain solution technique depicts the behavior of the E field below ground through parametric variations of frequency-independent (constant) ground parameters. The frequency-domain solution of the same equivalent circuit model of the E-field sensor uses ground parameters that are either frequency independent (constant) or frequency dependent to describe the transfer function, A, or sensor calibration of the sensor.

These two methods independently arrive at the solution of the transmitted E field below ground but both depend on σ and ε_r. The parameters σ and ε_r were the only ones adjusted to provide agreement between the calculated and measured E fields transmitted below ground. When the calculated and measured E fields are in good agreement for given σ and ε_r, a conclusion can be drawn from the results.

A flow chart of an indirect measure of below-ground E field, conductivity, and dielectric constant is shown in figure 1.

This report presents comparisons between calculated and measured transmitted E fields using both constant and frequency-dependent ground parameters.

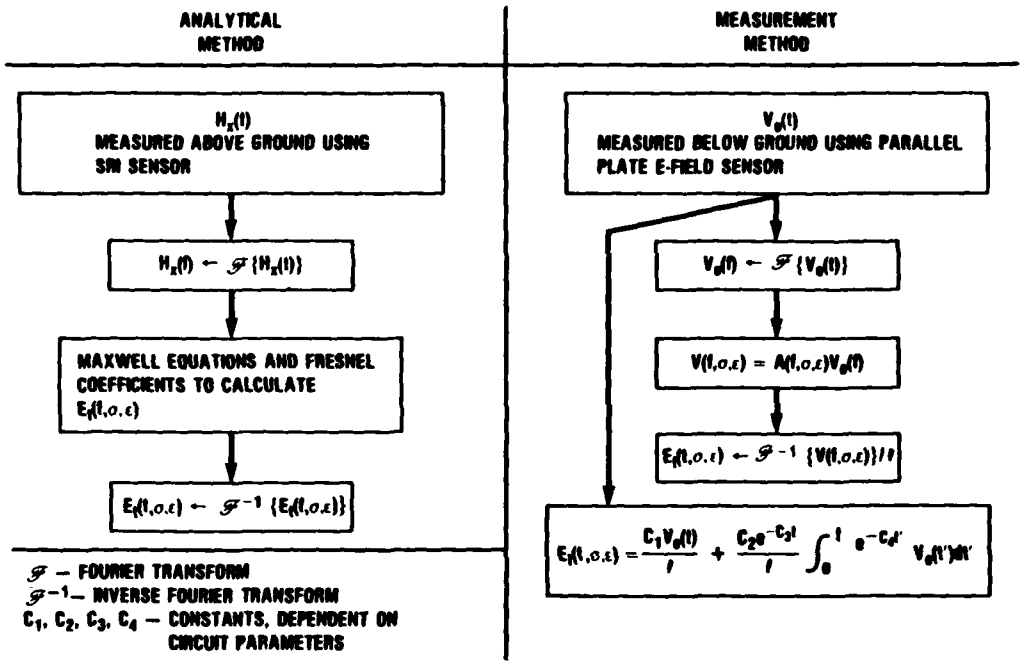

Figure 1. Flow chart of an indirect measure of below-ground E field, conductivity, and dielectric constant.

2. ANALYTICAL CALCULATION OF TRANSMITTED E FIELD

When an EMP is incident at the plane boundary of a linear, homogeneous, isotropic, and conducting medium, some of it is reflected and some is transmitted into the medium. The transmitted E field can be found with the use of Fresnel reflection and transmission coefficients.[1-3] The Fresnel coefficients are a function of the electrical properties of the ground and the incident angle of the electromagnetic wave. It is assumed in this study that the incident wave is a linearly polarized plane wave (of constant amplitude and phase) and the air/ground boundary is a semi-infinite plane.

The pertinent equations involve plane monochromatic waves (i.e., with single frequency) as directly derived from Maxwell's equations. Detailed derivations governing these equations can be found in works cited in the Selected Bibliography. Figure 2(a) diagrams the wave vectors of the incident, reflected, and transmitted waves used in this study. Figure 2(b) shows the conventional directions of electric and magnetic fields for horizontal polarization.

---

[1] *E. C. Jordan and K. G. Balmain, Electromagnetic Waves and Radiating Systems, Prentice-Hall, Inc., Englewood Cliffs, NJ (1968), 2nd ed.; ch 5, p 144 ff.*

[2] *J. D. Jackson, Classical Electrodynamics, John Wiley & Sons, Inc., New York (1962), ch 7, p 216 ff.*

[3] *M. Born and E. Wolf, Principles of Optics, Pergamon Press, Oxford (1970), fourth ed.; ch 1, p 40; ch 13, p 615 ff.*

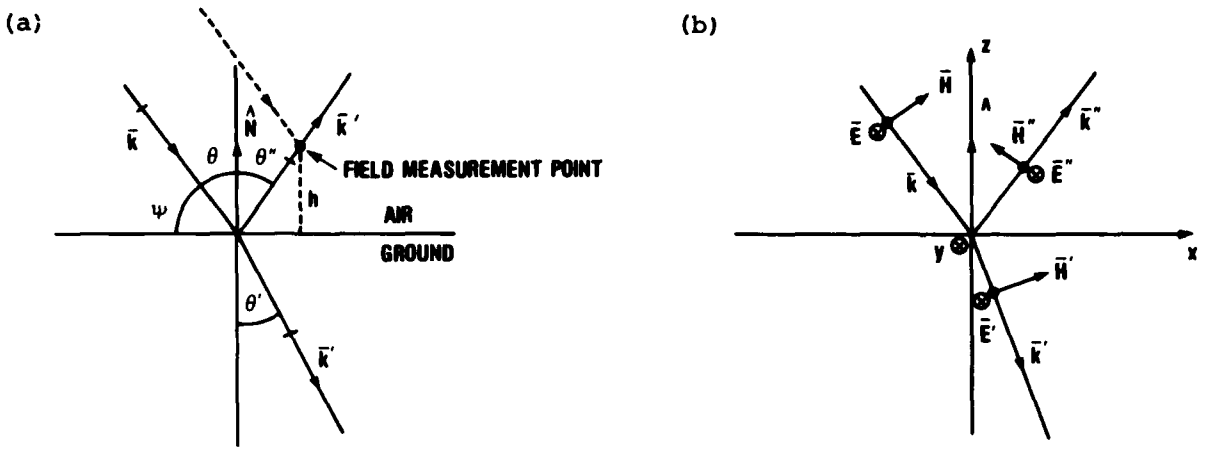

Figure 2. Waves and fields: (a) wave vectors of incident reflected and transmitted waves and (b) conventional directions of electric and magnetic fields for horizontal polarization.

The solution for the incident electric field above ground treated by Marx[4] is

$$E_o(\omega) = \{Z_o H_x(\omega)/[\sin\psi\ (1 - R_h(\omega)e^{-j\omega t_d})]\}\ |\sin(\omega t_d)/(\omega t_d)|^2 \quad . \qquad (1)$$

$E_o(\omega)$ is a function of the free-space wave impedance Z_o, the magnetic field $H_x(\omega)$, incident angle ψ, Fourier transform variable ω ($\omega = 2\pi f$), the Fresnel coefficient for horizontal polarization $R_h(\omega)$, and time delay t_d. The time delay describes the difference of arrival time between the incident and reflected pulses at the field measurement point above ground as shown in figure 2(a). The last term of equation (1) is a filter function that removes the singularities at

$$\omega t_d = k\pi \quad , \quad k = 1, 3, 5, \ldots$$

$R_h(\omega)$ is found to be

$$R_h(\omega) = \frac{\sin\psi - [\varepsilon_r - j(\sigma/\varepsilon_o\omega) - \cos^2\psi]^{1/2}}{\sin\psi + [\varepsilon_r - j(\sigma/\varepsilon_o\omega) - \cos^2\psi]^{1/2}} \quad , \qquad (2)$$

where ε_o is the dielectric permittivity of free space. The time delay is

$$t_d = \frac{2h\sin\psi}{c} \quad , \qquad (3)$$

where h is the height of the H-field sensor above ground (1 m) and c is the speed of light.

---

[4] *Egon Marx, Simulator Fields and Ground Constants, Harry Diamond Laboratories, HDL-TR-1785 (February 1977).*

The transmitted electric field $E_t(\omega)$ is

$$E_t(\omega) = T_h(\omega)e^{-\gamma d}E_o(\omega) \quad , \tag{4}$$

where d is the distance from the interface in the soil and γ is the propagation constant, defined as

$$\gamma = \left(-\omega^2\mu\varepsilon + j\omega\mu\sigma\right)^{1/2} \quad . \tag{5}$$

The transmission coefficient[5] $T_h(\omega)$ is

$$T_h(\omega) = \frac{2 \sin \psi}{\left\{\sin \psi + \left[\varepsilon_r - j\left(\sigma/\omega\varepsilon_o\right) - \cos^2\psi\right]^{1/2}\right\}} \quad . \tag{6}$$

The time-domain electric field $E_t(t)$ is numerically computed through an inverse Fourier transform[6] of equation (4). Finally, $E_t(t)$ is averaged over a 12-in. depth from 1 to 13 in. below the surface; the result is taken as the E field at 7 in. below the ground.

3. EXPERIMENTALLY MEASURED FIELDS

Field measurements were made at the REPS facility at the following locations (see fig. 3):

(a) test point 4 (TP4), close to the centerline at x = 800 ft and y = 82.5 ft south of the centerline, and

(b) test point 1 (TP1), off the centerline at x = 800 ft and y = 609 ft north of the centerline.

At each test point, two field measurements were taken: (1) the total magnetic field, $H_x(t)$, at 1 m above ground and (2) the transmitted component of the tangential E field averaged over a 12-in. depth from 1 to 13 in. below the surface.

The $H_x(t)$ was measured with a conventional Stanford Research Institute (SRI) cubical sensor box.[7] Figure 4 shows the measured $H_x(t)$ at TP1 and TP4.

---

[5] *Egon Marx, Reflected and Transmitted Fields for a Plane-Wave Pulse Incident on Conducting Ground, Harry Diamond Laboratories, HDL-TR-1740 (April 1976).*

[6] *Alfred G. Brandstein and Egon Marx, Numerical Fourier Transform, Harry Diamond Laboratories, HDL-TR-1748 (September 1976).*

[7] *B. C. Tupper, R. H. Stehle, and R. T. Wolfram, EMP Instrumentation Development, Stanford Research Institute, report 7990, under contract to Harry Diamond Laboratories, Contract DAAK-02-69-C-0674.*

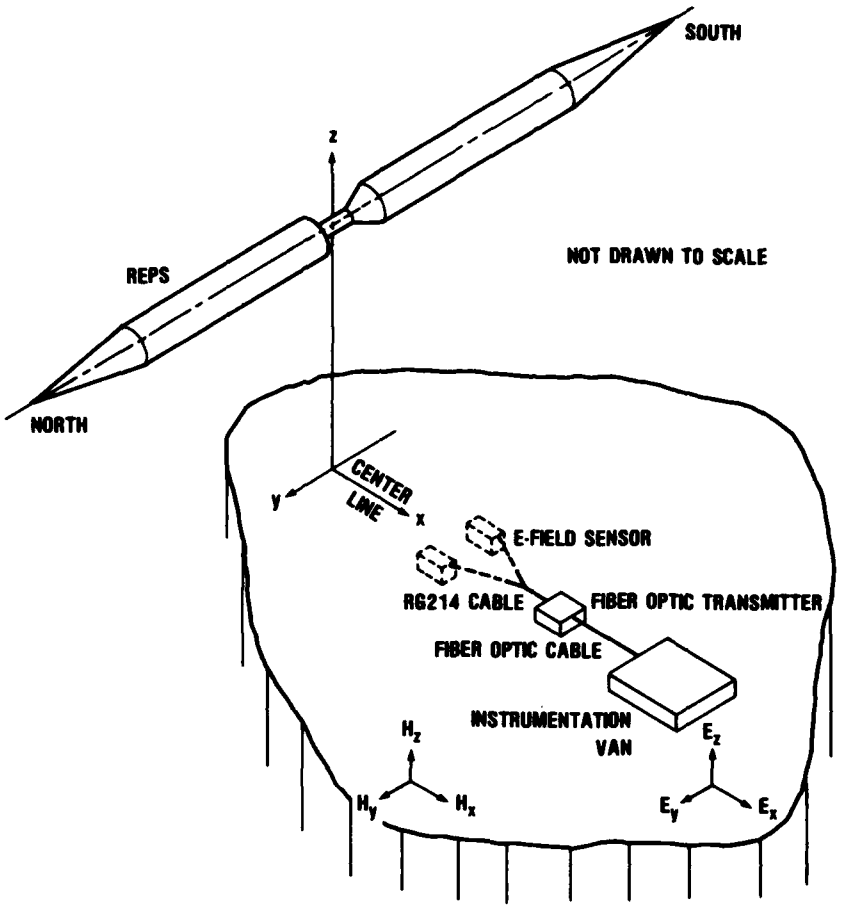

Figure 3. Isometric view of buried E-field sensor (dashed lines), measuring instruments, and REPS.

The transmitted E field was measured by the use of two buried parallel aluminum plates. These plates are 12 in. long × 12 in. wide × 1/4 in. thick. They were separated a distance ℓ of 1.75 in. at TP4 and 2.5 in. at TP1. In both cases the plates were inserted to achieve intimate ground contact. The voltage $V_o(t)$ generated across the plates by the field was measured by the use of a fiber-optic transmitter attached to the plate by an RG214, 50-Ω coaxial double-shielded cable. This cable was 1.75 ft long at TP4 and 3 ft long at TP1. The 50-Ω fiber-optic transmitter was connected to the instrumentation van remote-reading equipment by a fiber-optic cable and a 50-Ω fiber-optic receiver. The fiber-optic transmitter and receiver data link were designed and built by Jim Blackburn of HDL. Figure 5 shows the measured sensor voltage $V_o(t)$ at TP1 and TP4.

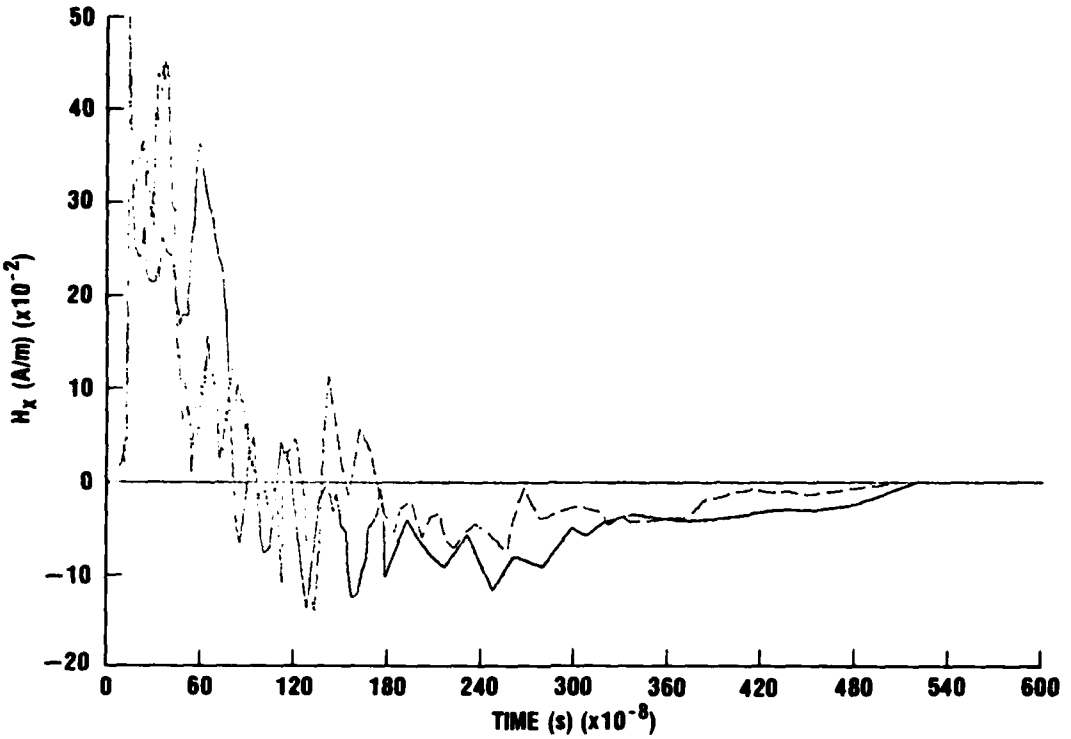

Figure 4. Measured $H_x(t)$ fields at TP1 (dashed line) and TP4 (solid line).

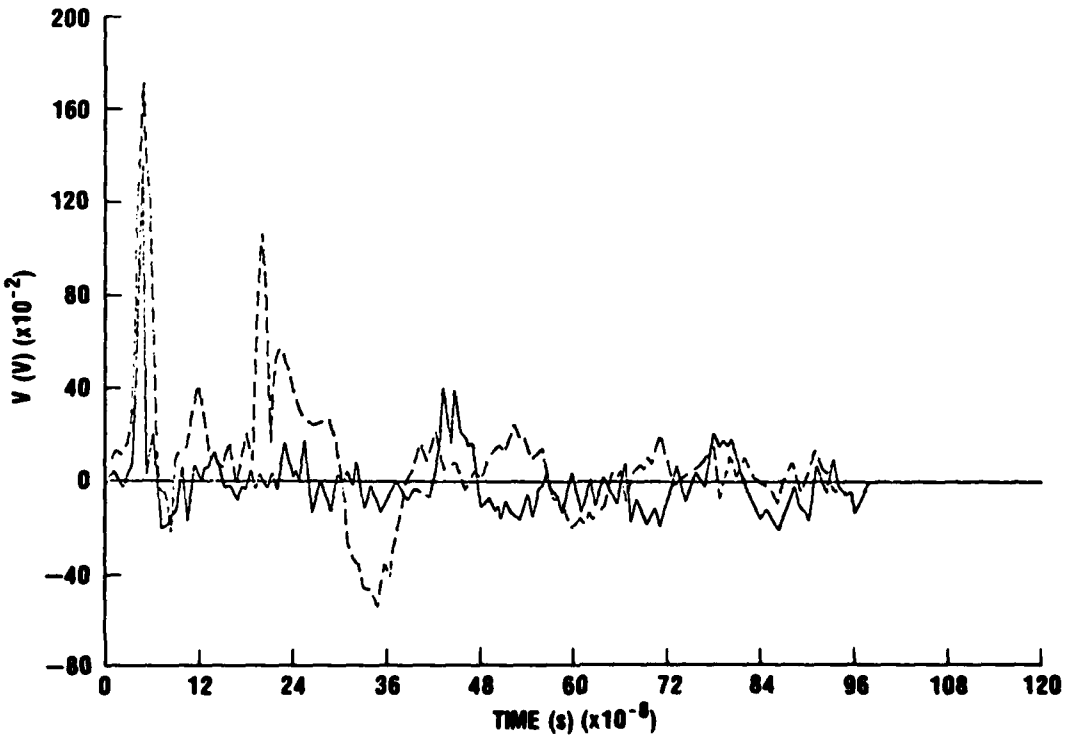

Figure 5. Measured sensor voltage $V_o(t)$ at TP1 (dashed line) and TP4 (solid line).

4. EFFECTS OF CONSTANT GROUND PARAMETERS--SENSOR CHARACTERIZATION

The E-field data are obtained from the measured voltage by the use of the equivalent circuit model as shown in figure 6. This model is described by Baum[8] as a short dipole antenna model. When time variations are slow enough that the short antenna approximation is valid, and assuming that the edge effects of the plates are not a significant factor, the equivalent circuit is used to represent the following relationship between the voltage through the load, $V_o(t)$, and the magnitude of the electric field, $E_t(t)$:

$$\left(C_s \frac{d}{dt} + G\right)\left[V(t) - V_o(t)\right] = \frac{V_o(t)}{R_L} + C_c \frac{dV_o(t)}{dt} \quad , \quad \text{for } t \geq 0 \quad . \tag{7}$$

Here $V(t) = E_t(t)\ell$, $G = 1/R_s = C_s\sigma/\varepsilon$, R_L is the load resistance, C_s = area, ε/ℓ is the sensor capacitance, and C_c is the cable capacitance. This is the same model for the E-field sensors used in Aurora with time-varying air conductivity.[9]

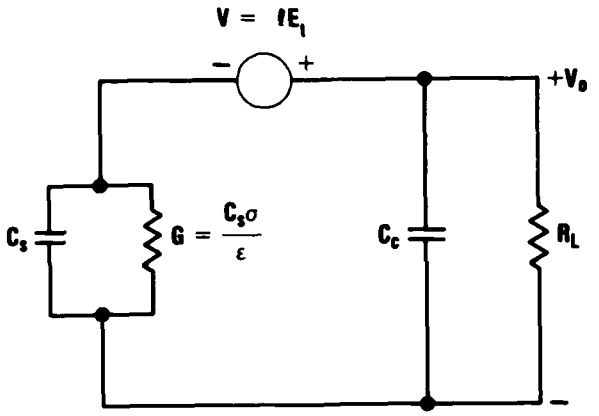

Figure 6. Equivalent circuit of E-field sensor.

The solution of differential equation (7) is composed of a complementary and a particular integral. In network terminology, these are also referred to as the natural, source-free, or transient response and the forced or steady-state response, respectively. Examination of equation (7) reveals that when R_L is large and C_c is zero, the source terms are zero and the solution is only complementary. Solving equation (7) by the method of variation of parameters, the solution for $E_t(t)$ is

---

[8] *C. E. Baum, Electromagnetic Pulse Sensor and Simulation Notes, Vol. 1, Air Force Weapons Laboratory, Note 13 (June 1970).*

[9] *Rolando P. Manriquez, George Merkel, William D. Scharf, and Daniel Spohn, Electrically-short Monopole Antenna Response in an Ionized Air Environment, Determination of Ionized Air Conductivity, IEEE Trans. Nucl. Sci. NS-26, 6 (December 1979), 5012-5018.*

$$E_t(t) = \frac{C_s + C_c}{\ell C_s} V_o(t) + \frac{C_s - GR_L C_c}{\ell R_L C_s^2} e^{-t/R_s C_s}$$

$$\times \int_0^t e^{-t'/R_s C_s} V_o(t')\, dt' \quad , \quad \text{for } t \geq 0 \quad . \tag{8}$$

Several important observations may be made from equation (8). When R_L is large and C_c is zero, and the transit time (ℓ/c) of the antenna model is long compared to the rise time τ of the incident pulse (i.e., $R_L C_s >> \tau$), the first term on the right-hand side of equation (8) dominates. In this case, the sensor can be regarded as an E-field sensor. On the other hand, when $R_L C_s << \tau$, the second term of equation (8) dominates and the sensor can be regarded as an $\dot{E}$-field sensor. Otherwise, the sensor can be described as a combination of an E- and $\dot{E}$-field sensor. The transmitted electric field $E_t(t)$ can be numerically computed from equation (8) or, alternatively, the voltage $V(t) = \ell E_t(t)$ can be obtained by solving the differential equation (7) by a Runge-Kutta or Gear method. The solutions of the first and second terms of equation (8) are shown in figure 7 at TP1 and figure 8 at TP4, respectively, with a constant σ = 0.007 mho/m and ε_r = 15.

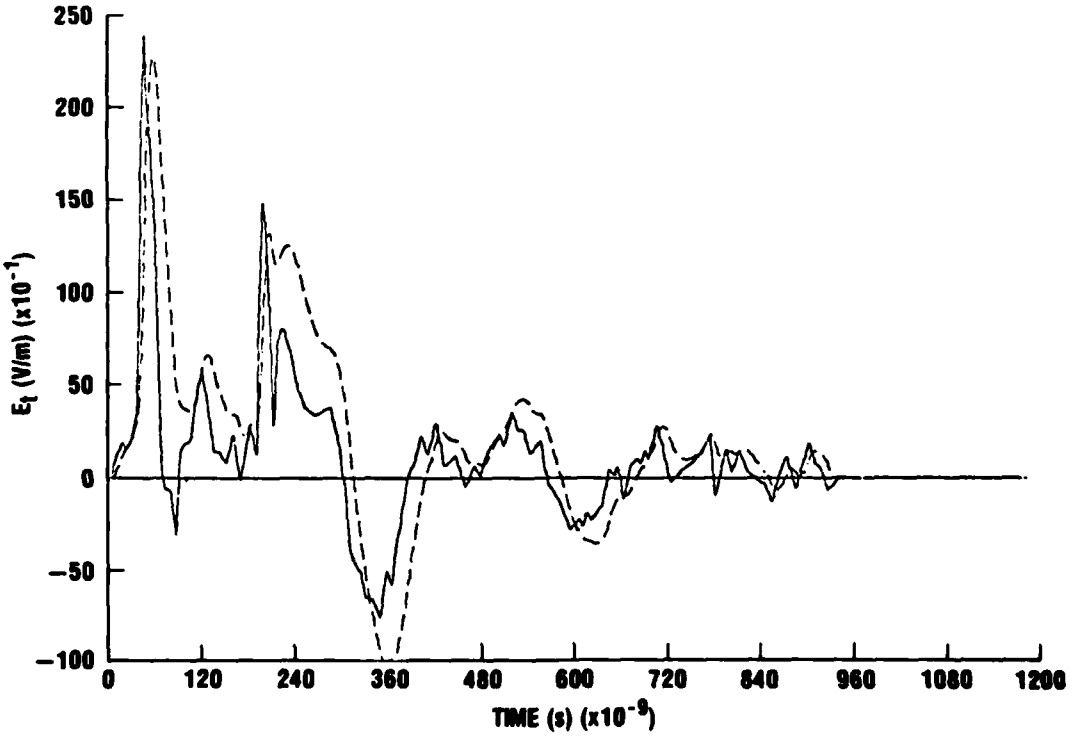

Figure 7. Results of first term (solid line) and second term (dashed line) of equation (8) at TP1 with σ = 0.007 mho/m and ε_r = 15.

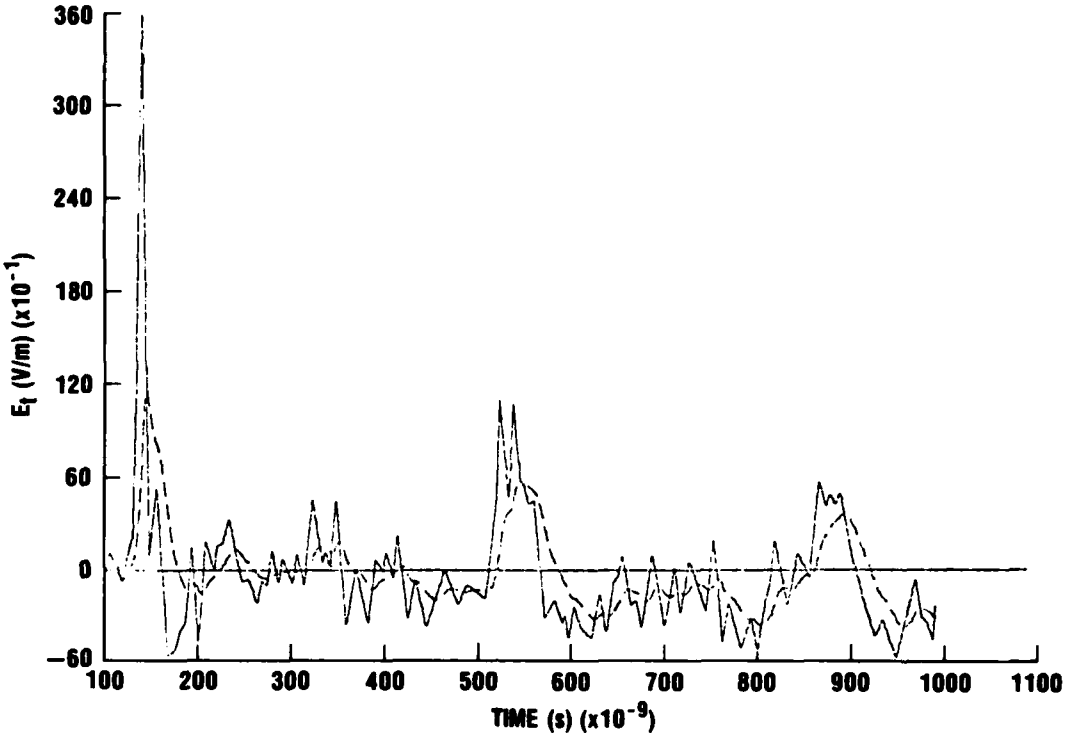

Figure 8. Results of first term (solid line) and second term (dashed line) of equation (8) at TP4 with σ = 0.007 mho/m and ε_r = 15.

Actual measurements of σ and ε_r were not available for the time this test was performed. However, previous data collected by the National Bureau of Standards (NBS) show that the ground conductivity is approximately 0.007 mho/m and the ε_r is 15 at 1 MHz. These data are discussed elsewhere[10] and measured for a limited frequency range. The results from equation (8) and the time-domain Fourier transform of equation (4) are shown in figures 9 to 13, at TP4, for σ varied with 0.001, 0.007, and 0.02 mho/m at ε_r = 15, and ε_r varied with 1, 15, and 80 at σ = 0.007 mho/m. Figure 14 shows the comparison between the results of equation (8) and the time-domain Fourier transform of equation (4), at TP1, for σ = 0.007 mho/m and ε_r = 15. The significance of the parametric variational effects to the expected values at the extreme is apparent. As σ and ε_r increase, the amplitude of the electric field decreases. The waveshapes at late times and low frequencies are somewhat altered at higher conductivities. The peak amplitude is particularly sensitive to the changes of the dielectric constant at higher frequencies.

[10] *Norman V. Hill, Effect of Frequency-Dependent Soil Parameters on Reflection Coefficients, Harry Diamond Laboratories, HDL-TR-2004 (December 1982).*

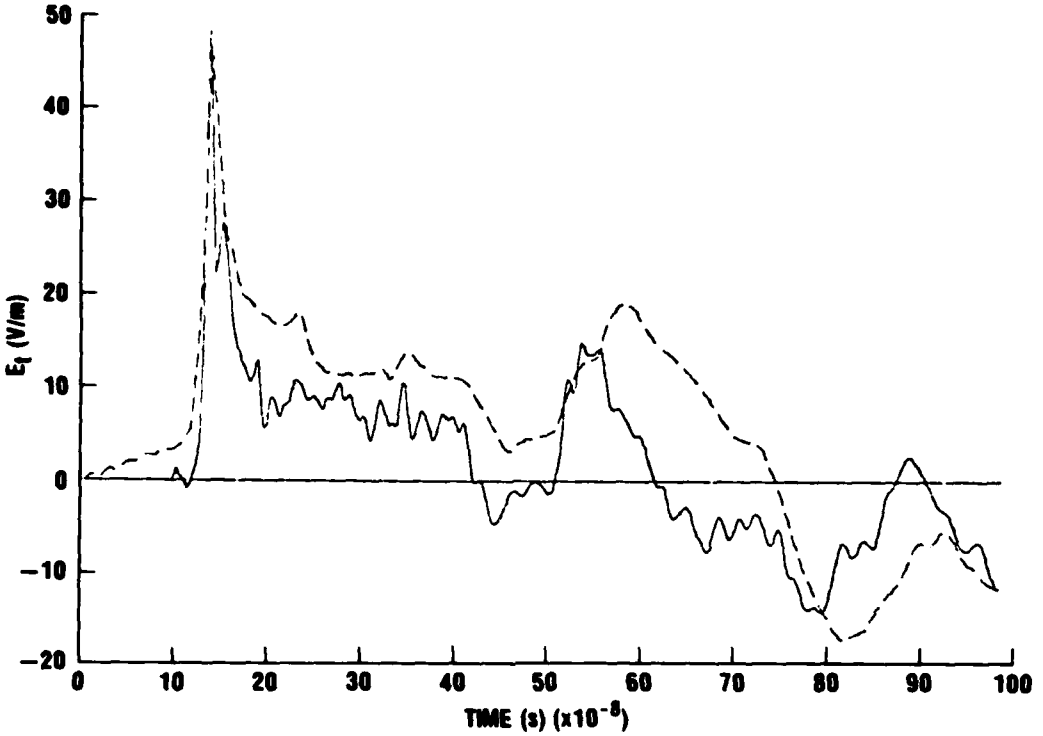

Figure 9. Comparison between calculated (dashed line) and measured (solid line) transmitted electric fields at TP4, with σ = 0.001 mho/m and ε_r = 15.

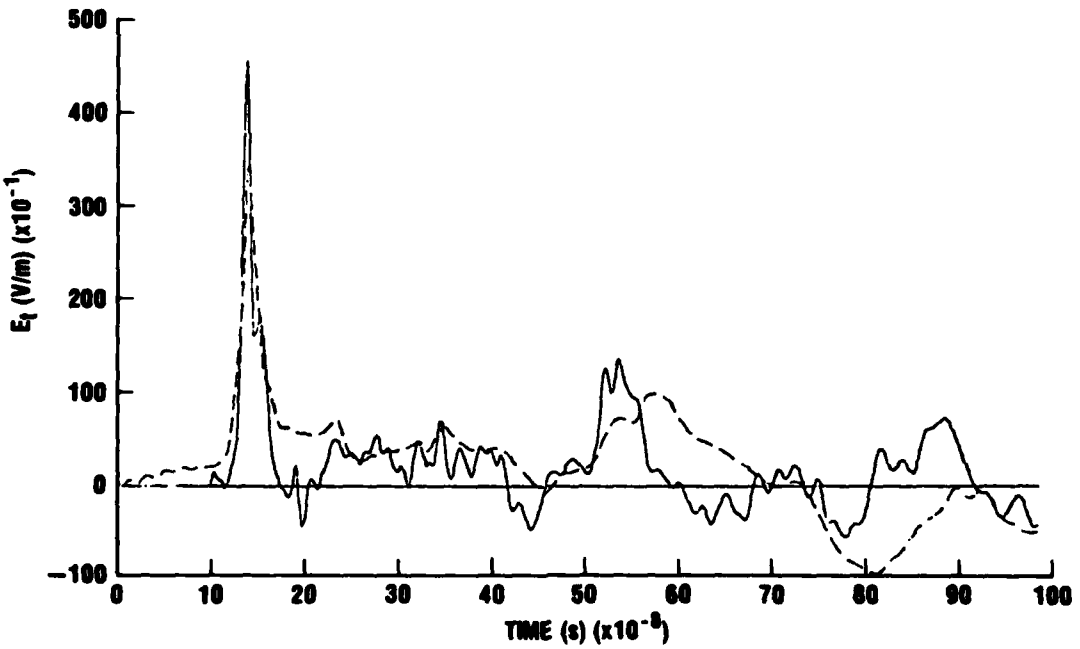

Figure 10. Comparison between calculated (dashed line) and measured (solid line) transmitted electric fields at TP4, with σ = 0.007 mho/m and ε_r = 15.

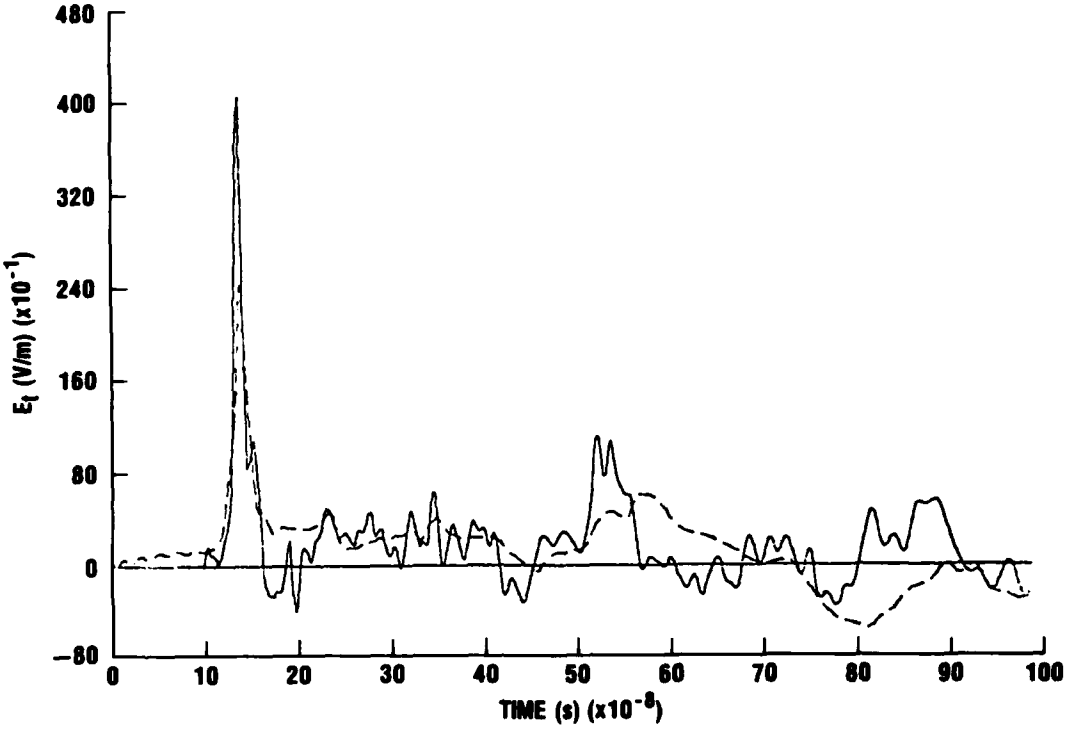

Figure 11. Comparison between calculated (dashed line) and measured (solid line) transmitted electric fields at TP4, with σ = 0.02 mho/m and ε_r = 15.

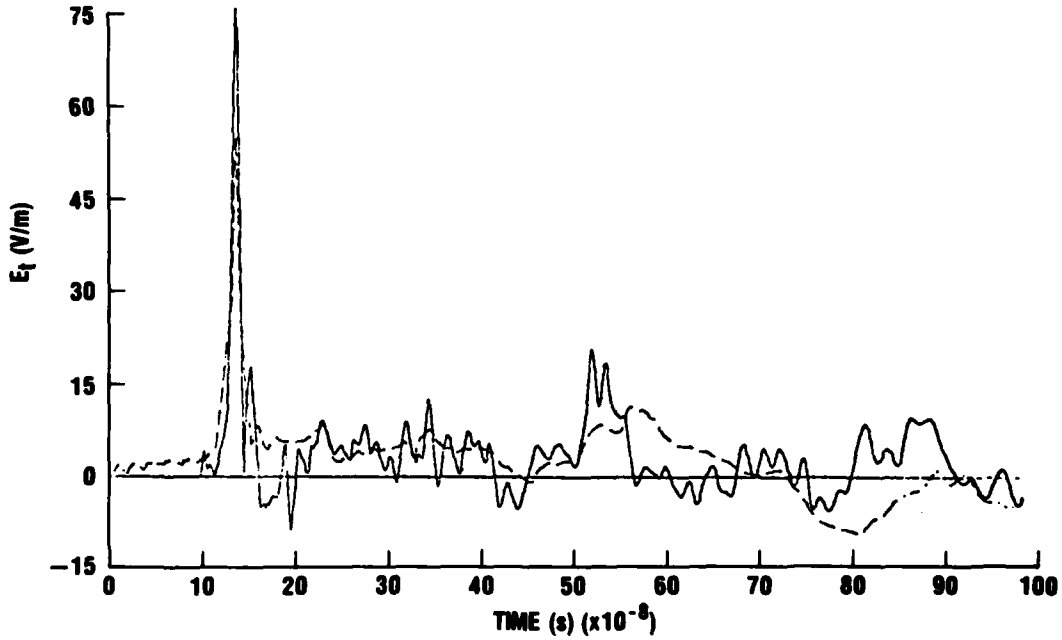

Figure 12. Comparison between calculated (dashed line) and measured (solid line) transmitted electric fields at TP4, with σ = 0.007 mho/m and ε_r = 1.

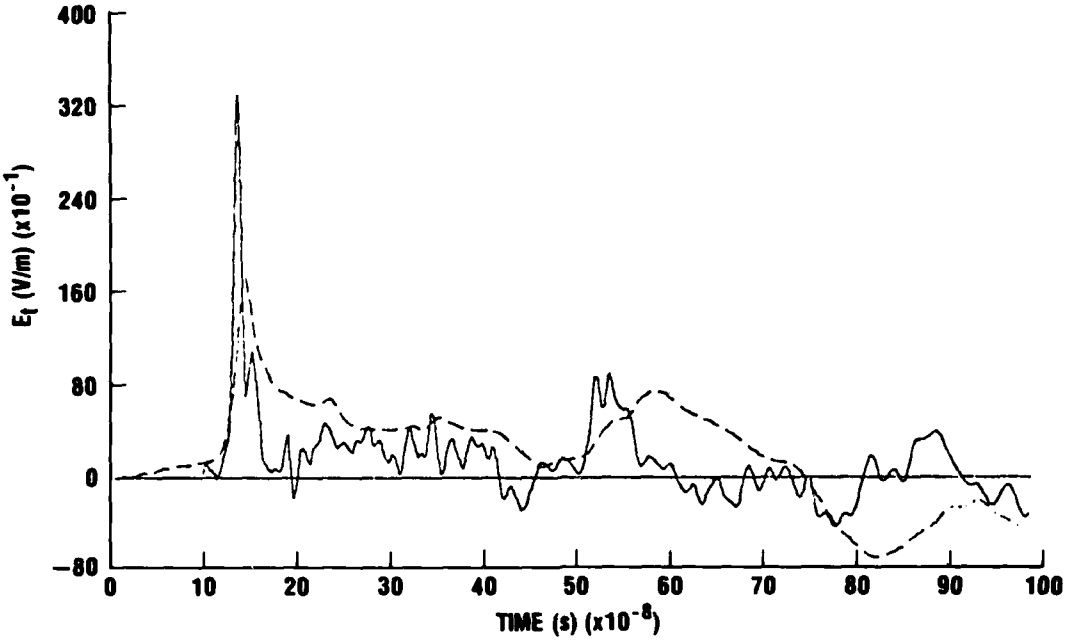

Figure 13. Comparison between calculated (dashed line) and measured (solid line) transmitted electric fields at TP4, with σ = 0.007 mho/m and ε_r = 80.

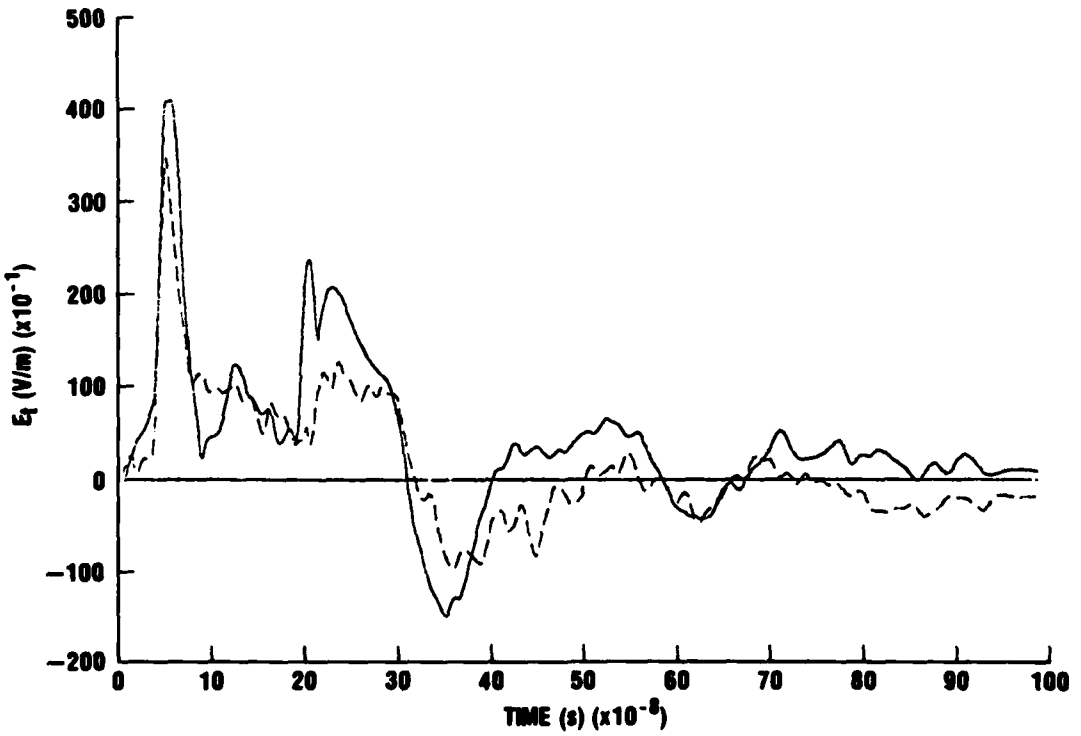

Figure 14. Comparison between calculated (dashed line) and measured (solid line) transmitted electric fields at TP1, with σ = 0.007 mho/m and ε_r = 15.

One of the unique features of the measuring system, depicted in figure 3, is the fiber-optic system. The advantage of implementing this system is to electrically isolate the E-field sensor from the instrumentation van, thereby eliminating the need for a long cable between the sensor and the van.

5. EFFECTS OF FREQUENCY-DEPENDENT GROUND PARAMETERS--SENSOR CALIBRATION

The use of constant (frequency-independent) values for σ and ε_r results in a sensor calibration (or transfer function) A that is a constant. This A can be used to determine the transmitted E field across the parallel-plate sensor as

$$E_t(\omega) = \frac{V_o(\omega)}{\ell} A \quad . \tag{9}$$

However, in reality, σ and ε_r are frequency dependent, and for larger variations of frequency, a more accurate calibration of the buried E-field sensor must include a frequency-dependent transfer function.

Let $A(\omega)$ be the transfer function of the buried E-field sensor as determined by taking the Laplace transform of equation (7) in the s-domain ($s = j\omega$). In general, the transfer function is a complex quantity and can be written as

$$A(\omega) = V(\omega)/V_o(\omega) \quad . \tag{10}$$

$A(\omega)$ is also stated in terms of magnitude and phase as

$$A(\omega) = |A(\omega)|e^{j\Phi(\omega)} \quad , \tag{11}$$

where $|A(\omega)|$ is the amplitude-response function and $\Phi(\omega)$ is the phase-shift function of the sensor. The transfer function depends on the circuit parameters as

$$A(\omega) = \frac{M + sB}{G + sC_s} \quad , \tag{12}$$

where $M = (1 + R_L G)/R_L$ and $B = C_s + C_c$. The amplitude-response function $|A(\omega)|$ is

$$|A(\omega)| = \left[1/(G^2 + \omega^2 C_s^2)\right]\left[(MG + \omega^2 BC_s)^2 + \omega^2(BG - C_s M)^2\right]^{1/2} \quad , \tag{13}$$

and the phase-shift function $\Phi(\omega)$ is

$$\Phi(\omega) = \tan^{-1}\frac{\omega(BG - C_s M)}{MG + \omega^2 BC_s} \quad . \tag{14}$$

The results for $|V_o(\omega)|$, $|V(\omega)|$, $|A(\omega)|$, and $\Phi(\omega)$ as a function of frequency are shown in figures 15 and 16 at TP4, respectively, for a constant σ = 0.007 mho/m and ϵ_r = 15. Ideally, this sensor should produce an amplitude frequency response that looks "flat" in the frequency band of interest and a phase shift that is a linear function of frequency. In other words, the spectrum of the measured input voltage $V(\omega)$ is identical to the spectrum of the output voltage $V_o(\omega)$ as expressed in equation (10). This means that the input voltage is passed undistorted by the measuring system. But for some cases, when the amplitude and phase frequency response are functions of σ and ϵ_r that vary with frequency and moisture content, the output voltage may be substantially different from the input. From these viewpoints, depending on the ground parameters, the sensor's transfer function could appreciably alter or distort the output voltage.

Finally, the "unfolded" measured transmitted electric field is

$$E_t(\omega) = A(\omega)V_o(\omega)/\ell \quad . \tag{15}$$

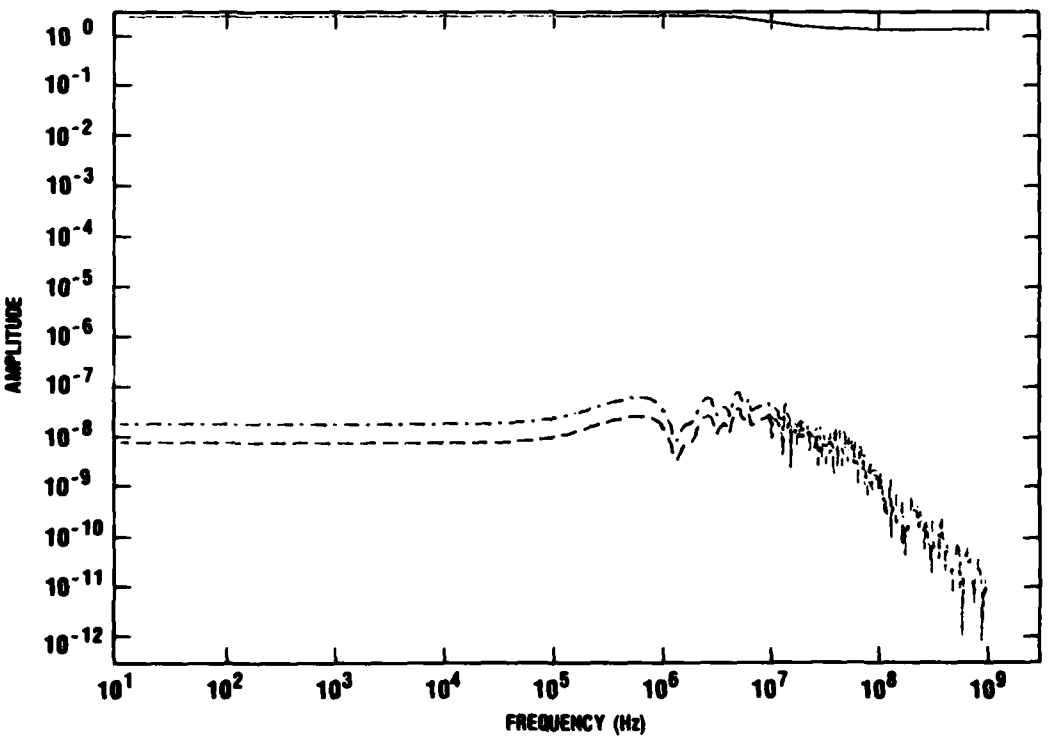

Figure 15. Magnitude of transfer function $A(\omega)$ (solid line), measured sensor voltage $V_o(\omega)$ (dashed line), and "unfolded" sensor voltage $V(\omega)$ (dash-dot line) at TP4, with σ = 0.007 mho/m and ϵ_r = 15.

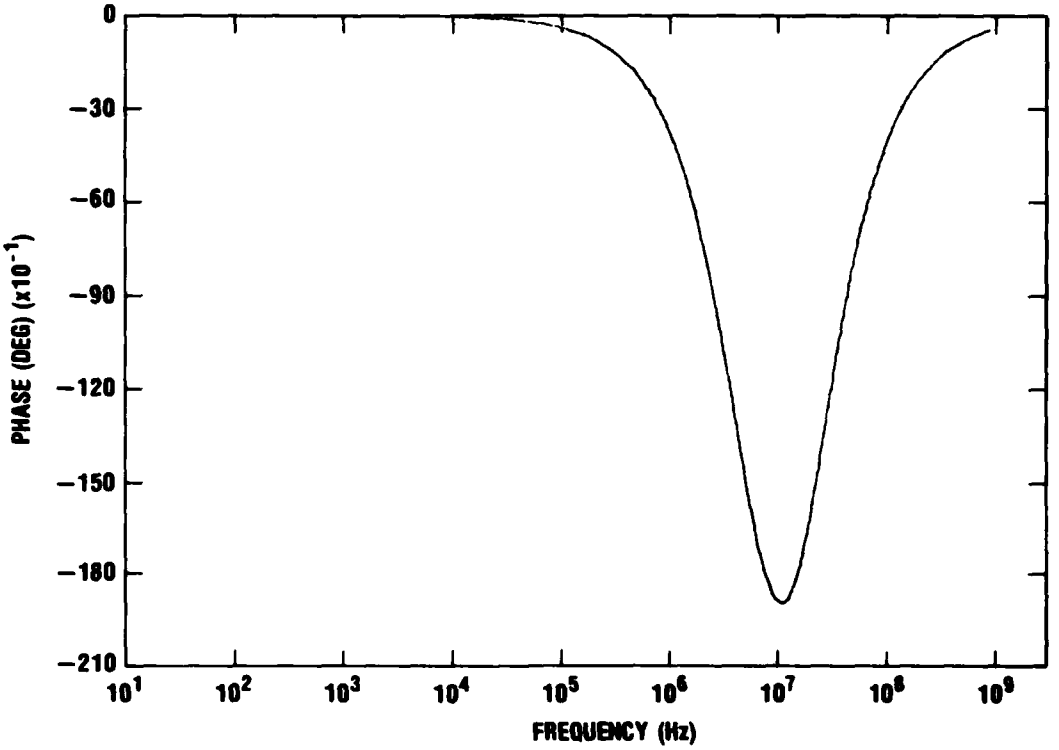

Figure 16. Phase shift function $\Phi(\omega)$ response of sensor at TP4, with σ = 0.007 mho/m and ε_r = 15.

Several studies have been conducted concerning the measurements and theoretical formulations of the electrical properties of the soil, namely, σ and ε_r as functions of frequency and moisture content. Longmire and Smith[11] developed a universal formula for σ and ε_r over the frequency range of 5 Hz to 3×10^{12} Hz, based on Scott's data[12] for soils and Wilkenfeld's data for some concrete and grout samples (Wilkenfeld's data can be found in Longmire and Smith[11]).

[11] *C. L. Longmire and K. S. Smith, A Universal Impedance for Soils, Mission Research Corp., Santa Barbara, CA, Contract No. DNA001-75-C-0094 (October 1975).*

[12] *J. H. Scott, Electrical and Magnetic Properties of Rock and Soils, Note 18, Electromagnetic Pulse Theoretical Notes, Air Force Weapons Laboratory, EMP 2-1 (April 1971); also U.S. Geological Survey Technical Letter, Special Project 16 (26 May 1966).*

The σ and ε_r derived from Longmire and Smith's "universal RC network model" are

$$\varepsilon_r = \varepsilon_\infty + \sum_{n=1}^{N} \frac{a_n}{1 + (f/f_n)^2} \quad \text{(relative)} \ , \tag{16}$$

$$\sigma = \sigma_o + 2\pi\varepsilon_o \sum_{n=1}^{N} a_n f_n \frac{(f/f_n)^2}{1 + (f/f_n)^2} \quad \text{(mho/m)} \ , \tag{17}$$

where

$N = 13$,

$\varepsilon_\infty = 5$,

f = frequency (Hz),

a_n = the constant coefficients (see table 1),

$f_n = F(P) f_n(10\%)$,

$f_n(10\%) = 10^{n-1}$ Hz,

$F(P) = (P/10)^{1.28}$,

P = water content (percent), and

$\sigma_o = 8.0 \times 10^{-3} \ (P/10)^{1.54}$ (mho/m).

Figure 17 shows the ground conductivity σ versus frequency for various volume percentages of water. Figure 18 shows the dielectric constant ε_r versus frequency for various volume percentages of water.

TABLE 1. COEFFICIENT a_n FOR UNIVERSAL SOIL (see eq (16) and (17))

n	a_n	n	a_n	n	a_n
1	3.4×10^6	6	1.33×10^2	11	9.80×10^{-1}
2	2.75×10^5	7	2.72×10^1	12	3.92×10^{-1}
3	2.58×10^4	8	1.25×10^1	13	1.73×10^{-1}
4	3.38×10^3	9	4.80		
5	5.26×10^2	10	2.17		

Because of the unavailability of Woodbridge's soil data over a wide range of frequency, it was necessary to implement Longmire and Smith's universal formula for σ and ε_r in the program. However, some old data taken by NBS for Woodbridge's soil show relatively low σ and ε_r; Hill[10] discusses these data. In the analysis, 10-percent soil moisture content, σ = 0.007 mho/m, and ε_r = 15 provided close agreement between calculated and measured transmitted E fields below ground. The results for $|V_o(\omega)|$, $|V(\omega)|$, $|A(\omega)|$, and $\Phi(\omega)$ with 10-percent moisture content at TP4 are shown in figures 19 and 20. The comparison between the inverse Fourier transform of the calculated transmitted electric field (eq (4)) and the "unfolded" measured transmitted electric field (eq (15)) using σ and ε_r dependent with frequency at 10- and 25-percent moisture content are shown in figures 21 and 22 at TP4, and figures 23 and 24 at TP1. Indeed, the transfer function of the sensor is highly sensitive to the electrical parameters of the soil.

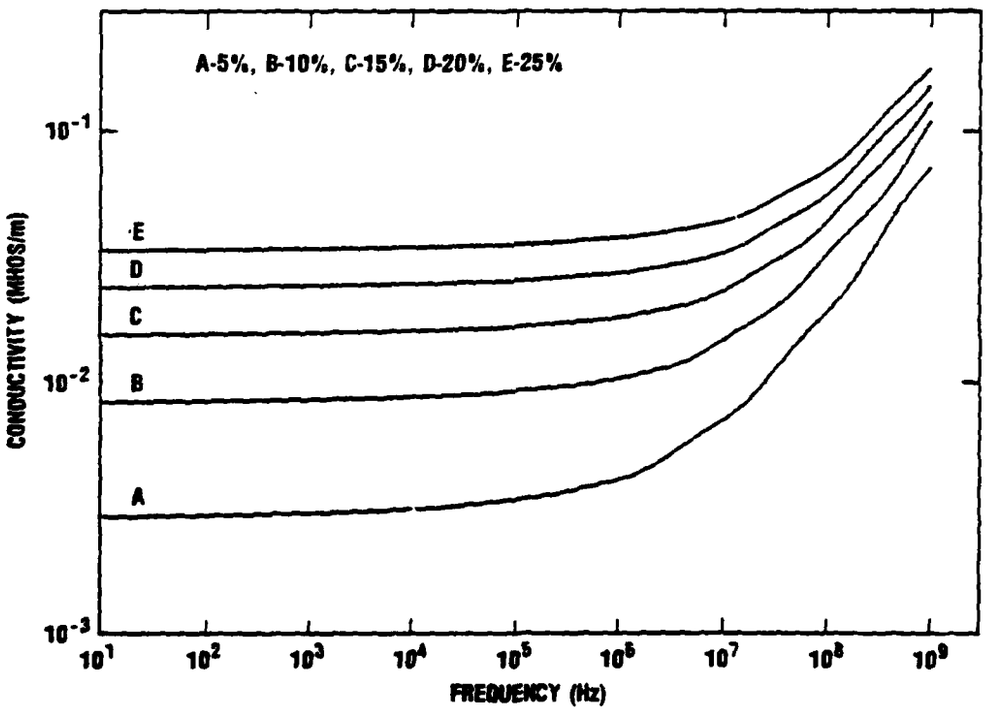

Figure 17. Conductivity versus frequency for various volume percentages of water.

[10] *Norman V. Hill, Effect of Frequency-Dependent Soil Parameters on Reflection Coefficients, Harry Diamond Laboratories, HDL-TR-2004 (December 1982).*

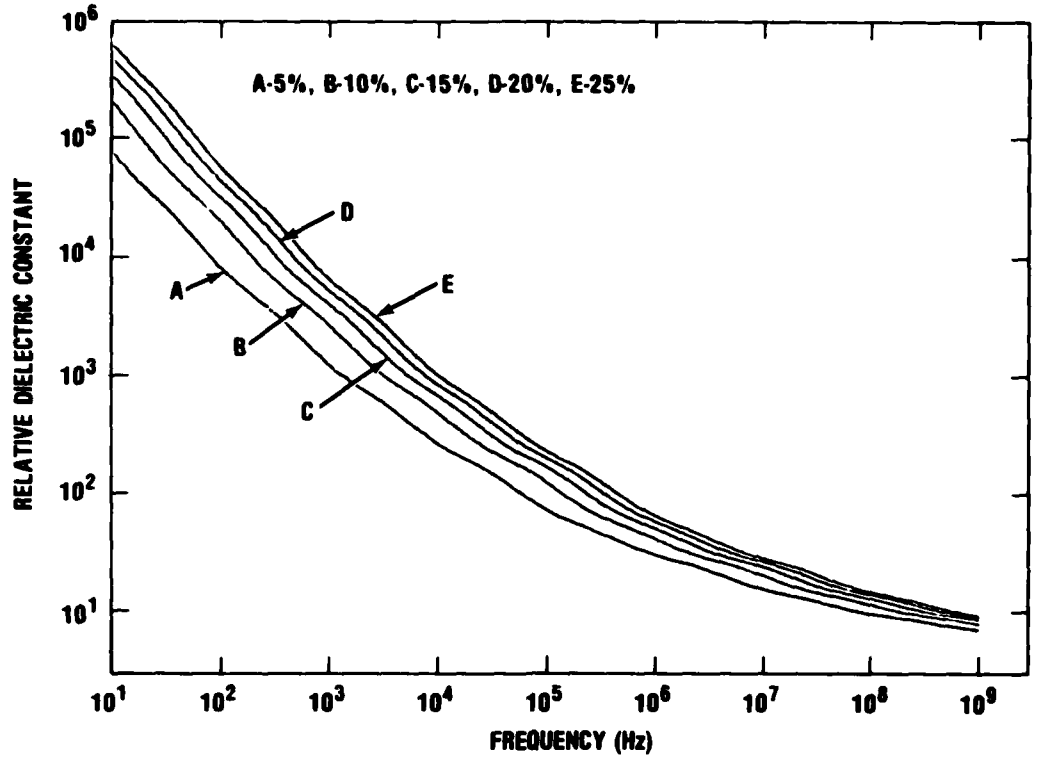

Figure 18. Dielectric constant versus frequency for various volume percentages of water.

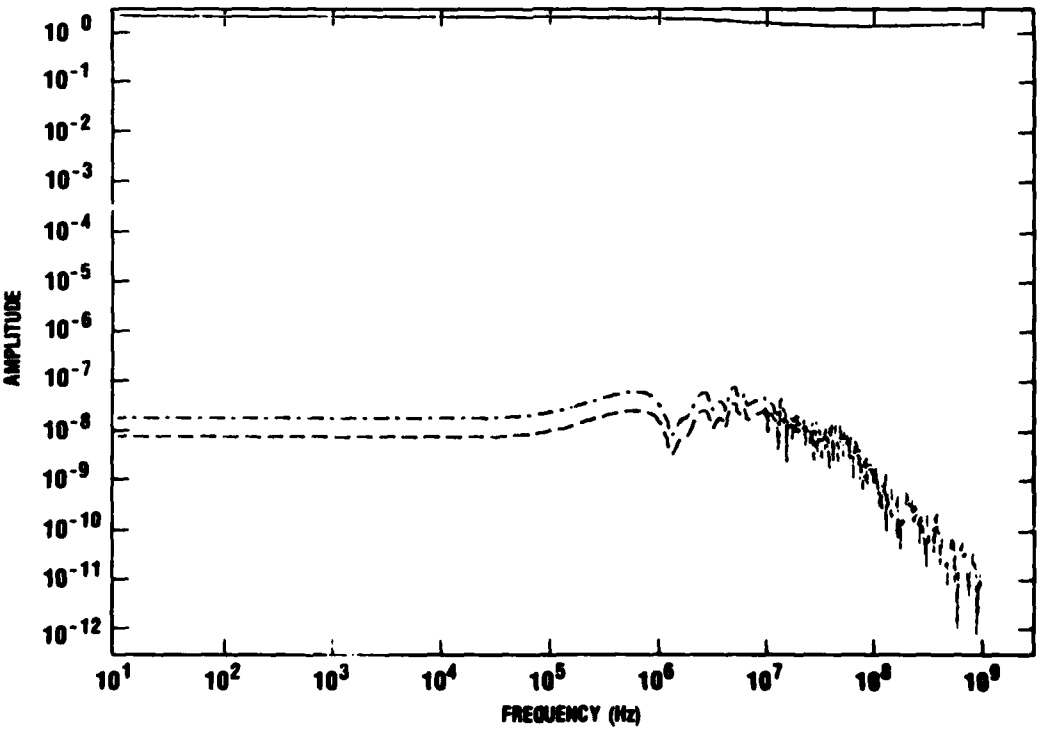

Figure 19. Magnitude of transfer function A(ω) (solid line), measured sensor voltage $V_o(\omega)$ (dashed line), and "unfolded" sensor voltage V(ω) (dash-dot line) at TP4, using Longmire's soil data (10-percent moisture content).

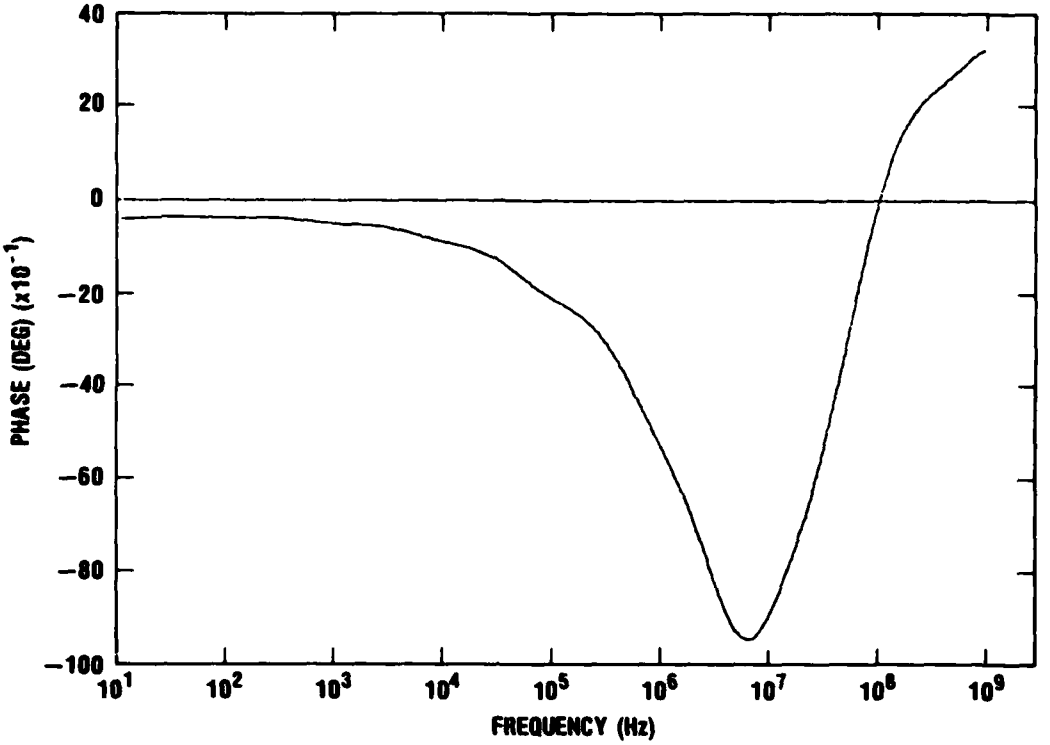

Figure 20. Phase shift function $\Phi(\omega)$ response of sensor at TP4, using Longmire's soil data (10-percent moisture content).

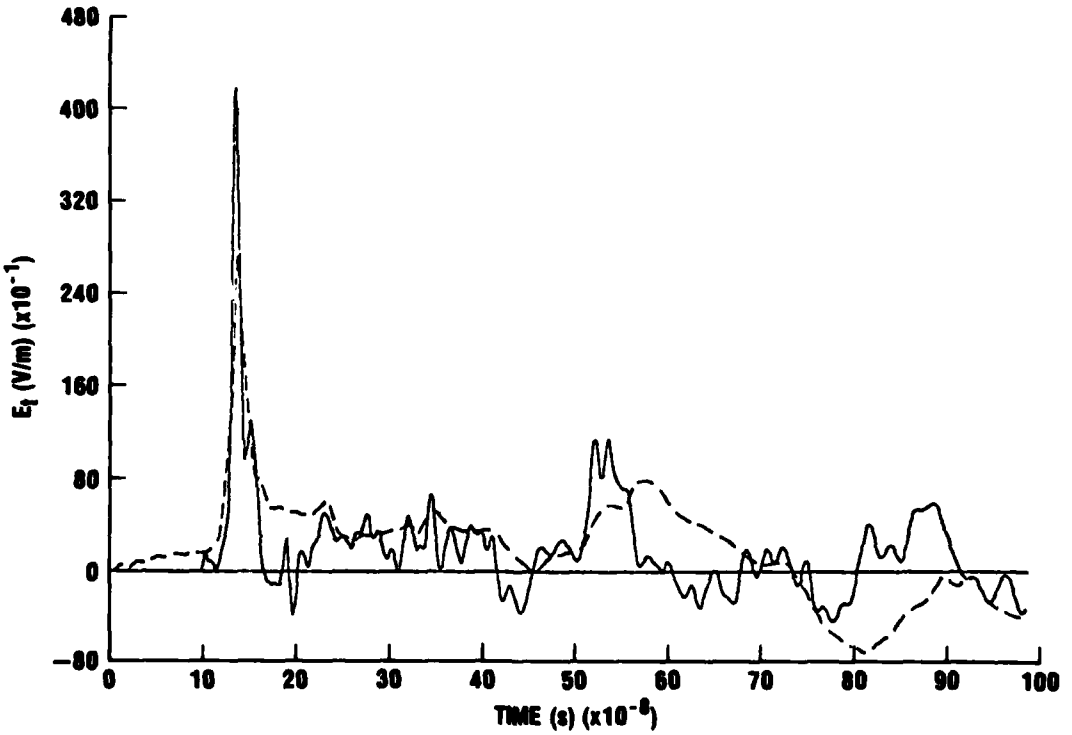

Figure 21. Comparison between calculated (dashed line) and measured (solid line) transmitted electric fields at TP4, using Longmire's soil data (10-percent moisture content).

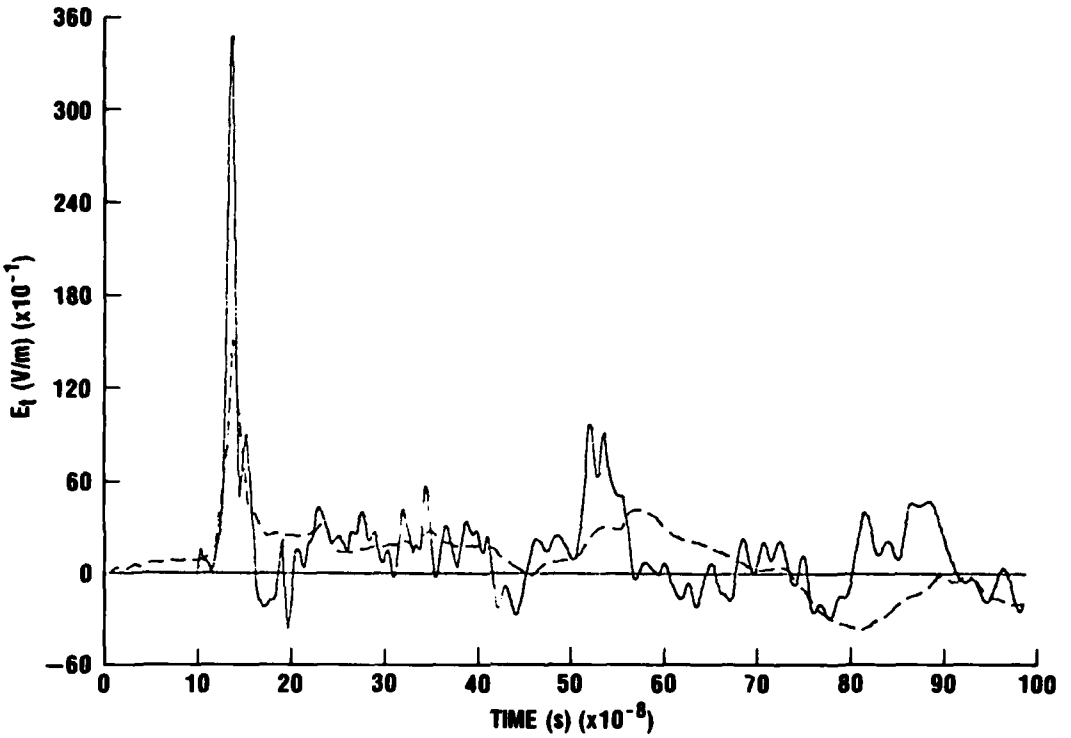

Figure 22. Comparison between calculated (dashed line) and measured (solid line) transmitted electric fields at TP4, using Longmire's soil data (25-percent moisture content).

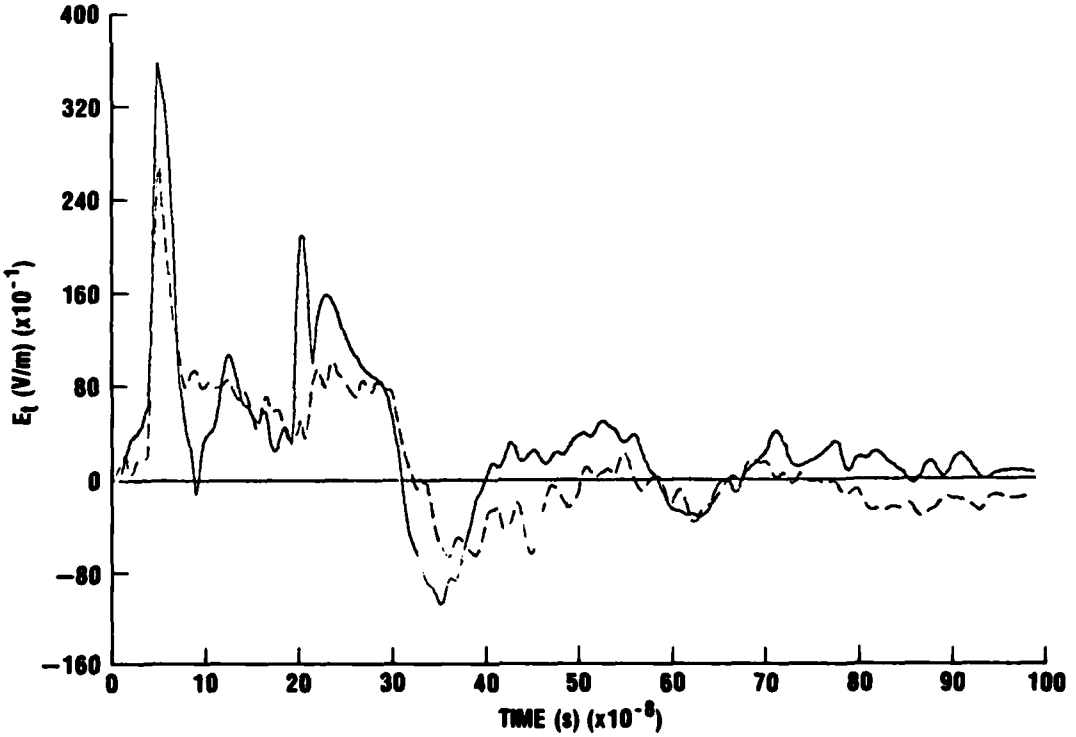

Figure 23. Comparison between calculated (dashed line) and measured (solid line) transmitted electric fields at TP1, using Longmire's soil data (10-percent moisture content).

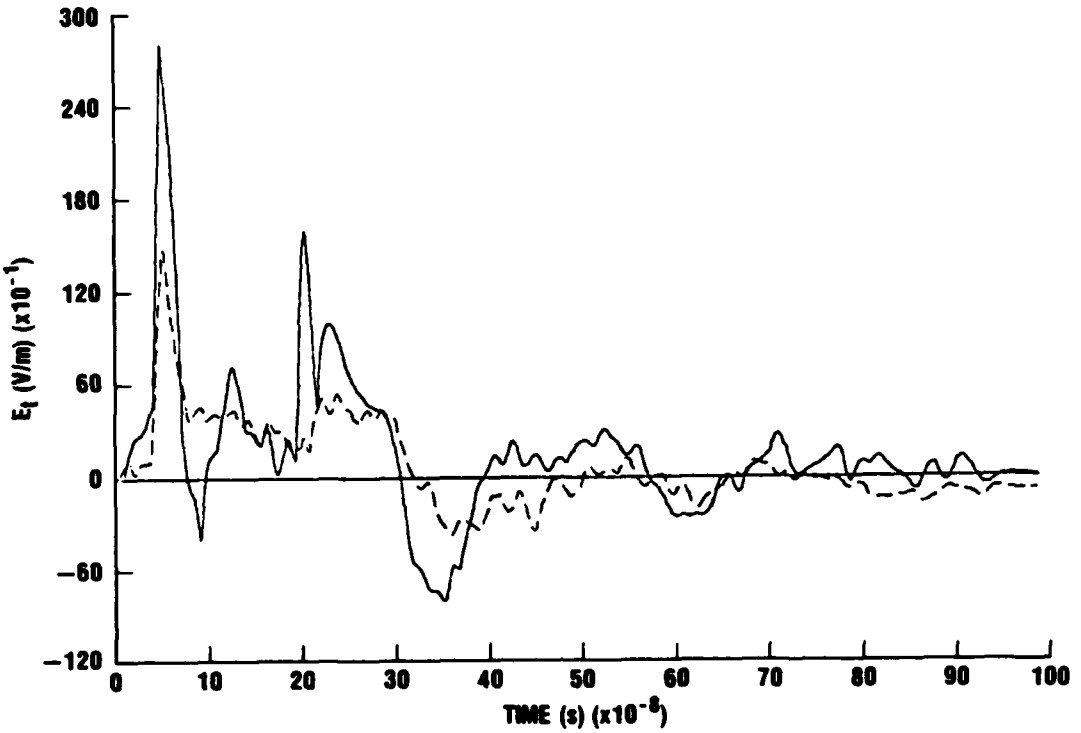

Figure 24. Comparison between calculated (dashed line) and measured (solid line) transmitted electric fields at TP1, using Longmire's soil data (25-percent moisture content).

6. CONCLUSION AND RECOMMENDATIONS

This paper documents an attempt to experimentally measure the E-field component of an EMP below ground and to compare the results to an analytical calculation. The results of equations (4) and (15) showed good agreement for 10-percent moisture content, constant $\sigma = 0.007$ mho/m, and $\varepsilon_r = 15$.

The measurements can be improved by the use of a differential-mode voltage probe to measure the transmitted E field. The RG214 cable can be removed and the sensor directly connected to the fiber-optic transmitter. Another improvement would be to accurately determine σ and ε_r over a wide range of frequency and depth at the same location where the fields were measured, and at about the same time. The availability of more soil data would reduce the uncertainty in the sensor calibration.

The assumption that the EMP was a plane wave over a homogeneous plane semi-infinite ground in the far-field radiation zone may be justified by the quality of the results. The transmitted E field vanishes at late times (>1 μs) but the transmitted H fields may not. Also not taken into account were the multiple reflection of the fields and the effects of dispersion due to the existence of different layers of strata below ground. These uncertainties can be resolved by measurement of the E and H fields at different depths below the air/ground interface.

Analysis has shown that it may be possible to indirectly measure σ and ϵ_r as a function of moisture content and frequency with the parallel-plate E-field sensor. The sensitivity of the sensor is demonstrated through the sensitivity (S) analysis of the equivalent circuit model of the sensor's response to varying moisture content (P), i.e., $S = \partial V/\partial P$ (see fig. 21 to 24).

Perhaps the most significant aspect of this effort is that, through an adequate calibration of the buried E-field sensor, a method now exists for the immediate and relatively easy indirect determination of ground conductivity and dielectric constant. This method, through the Fourier transform, could then be made available as frequency-domain data and applied as derived to all EMP coupling programs.

The curve-fitting equations (eq (16) and (17)) used by Longmire and Smith[11] that determined the ϵ_r and σ based on Scott and Wilkinfeld's data can be further modified by adjusting the necessary coefficients in the equations to obtain a closer correlation between the calculated and measured transmitted electric fields. A computer-aided optimization procedure[13] is needed to accomplish this task. This curve-fitting method can analytically improve the determination of the σ and ϵ_r for Woodbridge's soil.

The use of calibrated, shallow, buried parallel plates should be made part of all field-test system programs because it is a simple, inexpensive method of determining the soil conductivity at the same time that the experimental coupling data are collected on the system. Thus, a conductivity measurement made at the beginning of each test day can be used to predict the signal levels expected. And, in addition, an accurate evaluation of experimentally collected data can then be used by the analyst to predict the levels of induced signals for any conditions of soil.

Future efforts will be to explore ways of improving the measurement method by (1) the determination of the effects of RG214 cable on the measurement, (2) an independent direct measurement of σ, ϵ_r, and P by whatever means, (3) the use of a different buried sensor (dipole, magnetic loop, two parallel cylinders, two parallel spheres, etc), and (4) the measurement of conduction current density (σE_t) below the ground using the parallel-plate sensor. This last measurement can be performed by connecting a large resistor between the sensor and a short RG214 cable. In series with the cable will be an impedance-matching device. This device will match the high-impedance sensor system (sensor and resistor) to the low-impedance data-link system (cable and fiber-optic system). The use of an impedance-matching device makes it possible to directly measure the induced sensor voltage. The signal propagated below the ground will be produced by the REPS.

---

[11] *C. L. Longmire and K. S. Smith, A Universal Impedance for Soils, Mission Research Corp., Santa Barbara, CA, Contract No. DNA001-75-C-0094 (October 1975).*

[13] *R. Fletcher and M. J. D. Powell, A Rapidly Convergent Descent Method for Minimization, Computer J. 6 (1963), 163.*

A fifth way to improve the method is by the measurement of displacement current density--$\epsilon(dE_t/dt)$--below the ground. This measurement can be performed by covering one of the plates with a thin insulator (e.g., plastic) and burying these plates below the ground. The results of all these measurements will further validate the results obtained from the existing analytical techniques employed in this report.

A conclusion reached as a result of this study is that the equivalent circuit model of the sensor is an adequate model for REPS field rise times and typical ground parameters. The modeled sensor system performed well and provided physical insight to the problem. The transfer functions were evaluated directly from the circuit model and showed the characteristic response of the sensor.

The determination of the E field below ground due to an incident EMP field is summarized as follows:

(1) The H field above ground was measured and used to calculate the transmitted E field with the aid of Maxwell's equations and the Fresnel coefficients.

(2) The induced voltage across the parallel-plate sensor was measured and "unfolded" in two ways:

(a) time-domain formulation of the equivalent circuit model of the E-field sensor using constant ground parameters, and

(b) frequency-domain formulation of the same equivalent circuit model using ground parameters dependent on frequency and moisture content.

Finally, the applied conceptual and measurement scheme showed satisfactory results and provided vital information about EMP field sensors and the electrical properties of the conducting ground.

LITERATURE CITED

(1) E. C. Jordan and K. G. Balmain, Electromagnetic Waves and Radiating Systems, Prentice-Hall, Inc., Englewood Cliffs, NJ (1968), 2nd ed.; ch 5, p 144 ff.

(2) J. D. Jackson, Classical Electrodynamics, John Wiley & Sons, Inc., New York (1962), ch 7, p 216 ff.

(3) M. Born and E. Wolf, Principles of Optics, Pergamon Press, Oxford (1970), fourth ed.; ch 1, p 40; ch 13, p 615 ff.

(4) Egon Marx, Simulator Fields and Ground Constants, Harry Diamond Laboratories, HDL-TR-1785 (February 1977).

(5) Egon Marx, Reflected and Transmitted Fields for a Plane-Wave Pulse Incident on Conducting Ground, Harry Diamond Laboratories, HDL-TR-1740 (April 1976).

(6) Alfred G. Brandstein and Egon Marx, Numerical Fourier Transform, Harry Diamond Laboratories, HDL-TR-1748 (September 1976).

(7) B. C. Tupper, R. H. Stehle, and R. T. Wolfram, EMP Instrumentation Development, Stanford Research Institute, report 7990, under contract to Harry Diamond Laboratories, Contract DAAK-02-69-C-0674.

(8) C. E. Baum, Electromagnetic Pulse Sensor and Simulation Notes, Vol. 1, Air Force Weapons Laboratory, Note 13 (June 1970).

(9) Rolando P. Manriquez, George Merkel, William D. Scharf, and Daniel Spohn, Electrically-short Monopole Antenna Response in an Ionized Air Environment, Determination of Ionized Air Conductivity, IEEE Trans. Nucl. Sci. NS-26, 6 (December 1979), 5012-5018.

(10) Norman V. Hill, Effect of Frequency-Dependent Soil Parameters on Reflection Coefficients, Harry Diamond Laboratories, HDL-TR-2004 (December 1982).

(11) C. L. Longmire and K. S. Smith, A Universal Impedance for Soils, Mission Research Corp., Santa Barbara, CA, Contract No. DNA001-75-C-0094 (October 1975).

(12) J. H. Scott, Electrical and Magnetic Properties of Rock and Soils, Note 18, Electromagnetic Pulse Theoretical Notes, Air Force Weapons Laboratory, EMP 2-1 (April 1971); also U.S. Geological Survey Technical Letter, Special Project 16 (26 May 1966).

(13) R. Fletcher and M. J. D. Powell, A Rapidly Convergent Descent Method for Minimization, Computer J. 6 (1963), 163.

SELECTED BIBLIOGRAPHY

Baum, C. E., The Reflection of Pulsed Waves from the Surface of a Conducting Dielectric, Air Force Weapons Laboratory, EMP Theoretical Note 25 (1967).

King, R. W. P., and C. W. Harrison, Jr., J. Appl. Phys. 39 (1968), 4444.

Klebers, Janis, Time Domain Analysis of the Electromagnetic Field in the Presence of a Finitely Conducting Surface, Proceedings: Department of the Army Security Agency EMP Technical Conference (1969), p 4-1.

Kraichman, M. B., Handbook of Electromagnetic Propagation in Conducting Media, Headquarters Naval Material Command, NAVMATP-2302 (1970).

Marx, Egon, Simulator Fields and Ground Constants, Harry Diamond Laboratories, HDL-TR-1785 (February 1977).

Marx, Egon, Reflected and Transmitted Fields for a Plane-Wave Pulse Incident on Conducting Ground, Harry Diamond Laboratories, HDL-TR-1740 (April 1976).

Messier, M. A., The Effect of Ground Reflection on Observed EMP Waveforms, Topical Report, Mission Research Corp., Santa Barbara, CA (1974).

Monroe, Richard L., J. Appl. Phys. 40 (1969), 3526; 41 (1970), 4820.

Vance, E. F., Coupling to Shielded Cables, John Wiley & Sons, Inc. (1978).

Wait, J. R., and C. Froese, J. Geophys. Res. 60 (1955), 97.

DISTRIBUTION

ADMINISTRATOR
DEFENSE TECHNICAL INFORMATION CENTER
CAMERON STATION, BUILDING 5
ATTN DTIC-DDA (12 COPIES)
ALEXANDRIA, VA 22314

NATIONAL COMMUNICATIONS SYSTEM
DEPARTMENT OF DEFENSE
OFFICE OF THE MANAGER
ATTN NCS-TS, D. BODSON (150 COPIES)
WASHINGTON, DC 20305

ASSISTANT TO THE SECRETARY OF DEFENSE
ATOMIC ENERGY
ATTN EXECUTIVE ASSISTANT
WASHINGTON, DC 20301

DIRECTOR
DEFENSE COMMUNICATIONS AGENCY
ATTN CODE B410
ATTN CODE B430
ATTN CODE J300, KNAPP
WASHINGTON, DC 20305

DIRECTOR
COMMAND CONTROL ENGINEERING CENTER
ATTN C-661, DR. T. TRINKLE
ATTN G-630, R. LIPP
WASHINGTON, DC 20305

DIRECTOR
DEFENSE COMMUNICATIONS ENGINEERING CENTER
ATTN CODE R400
ATTN CODE R123, TECH LIB
ATTN CODE R111, SICA
1860 WIEHLE AVENUE
RESTON, VA 22090

ASSISTANT CHIEF OF STAFF FOR
INFORMATION MANAGEMENT
COMMAND SYSTEMS INTEGRATION OFFICE
ATTN DAMO-C4Z, COL. D. GRIGGS
THE PENTAGON
WASHINGTON, DC 20301

DIRECTOR
DEFENSE INTELLIGENCE AGENCY
ATTN DB-4C2, D. SPOHN
WASHINGTON, DC 20301

CHAIRMAN
JOINT CHIEFS OF STAFF
ATTN J-3
ATTN C3S
WASHINGTON, DC 20301

DIRECTOR DEFENSE NUCLEAR AGENCY
ATTN NATA
ATTN RAEV
ATTN DDST
ATTN RAEE
ATTN TITL
WASHINGTON, DC 20305

OFFICE OF UNDERSECRETARY OF DEFENSE
RESEARCH & ENGINEERING
DMSSO
2 SKYLINE PLACE
SUITE 1403
5203 LEESBURG PIKE
FALLS CHURCH, VA 22041

UNDER SECY OF DEF FOR RSCH & ENGRG
DEPARTMENT OF DEFENSE
ATTN STRATEGIC & SPACE SYS 9OSO RM 3E129
ATTN STRAT & THEATER NUC FORCES
WASHINGTON, DC 20301

DEPUTY DIRECTOR FOR THEATRE/TACTICAL C3
SYSTEMS
JOINT STAFF
WASHINGTON, DC 20301

COMMANDER-IN-CHIEF
US FORCES, EUROPE
ATTN ECC3S
APO, NY 09128

ASSISTANT CHIEF OF STAFF FOR
AUTOMATION & COMMUNICATIONS
ATTN DAMO-C4T
ATTN DAMO-C4S
DEPARTMENT OF THE ARMY
WASHINGTON, DC 20360

US ARMY BALLISTIC RESEARCH LABORATORY
ATTN DRDAR-TSB-S (STINFO)
ABERDEEN PROVING GROUND, MD 21005

COMMANDER
US ARMY COMMUNICATIONS COMMAND
ATTN CC-OPS-WR, O. P. CONNELL
FT HUACHUCA, AZ 85613

COMMANDER
US ARMY COMM-ELEC INSTAL AGENCY
ATTN CCC-CE-TS
FT HUACHUCA, AZ 85613

CHIEF
US ARMY COMMUNICATIONS SYS AGENCY
DEPARTMENT OF THE ARMY
ATTN TECHNICAL DIRECTOR
FT MONMOUTH, NJ 07703

COMMANDER
5TH SIGNAL COMMAND HEADQUARTERS
ATTN DCS OPS, K. MILLER
APO, NY 09056

US ARMY ELECTRONICS TECHNOLOGY
& DEVICES LABORATORY
ATTN DELET-DD
FT MONMOUTH, NJ 07703

US ARMY ENGINEER DIV HUNTSVILLE
DIVISION ENGINEER
ATTN HNDED FD, T. BOLT
PO BOX 1600
HUNTSVILLE, AL 35807

COMMANDER
US ARMY MATERIEL COMMAND
ATTN DRCRE
ATTN DRCDE
5001 EISENHOWER AVE
ALEXANDRIA, VA 22333-0001

DIRECTOR
US ARMY MATERIEL SYSTEMS ANALYSIS
ACTIVITY
ATTN DRXSY-MP, LIBRARY
ABERDEEN PROVING GROUND, MD 21005

COMMANDER
US ARMY MISSILE & MUNITIONS
CENTER & SCHOOL
ATTN ATSK-CTD-F
REDSTONE ARSENAL, AL 35809

COMMANDER
US ARMY NUCLEAR & CHEMICAL AGENCY
ATTN MONA-WE
7500 BACKLICK RD
SPRINGFIELD, VA 22150

DEP CH OF STAFF FOR RSCH DEV & ACQ
DEPARTMENT OF THE ARMY
ATTN DAMA-CSS-N
WASHINGTON, DC 20310

COMMANDER
US ARMY RSCH & STD GP (EUR)
ATTN CHIEF, PHYSICS & MATH BRANCH
FPO NEW YORK 09510

CHIEF
US ARMY SATELLITE COMMUNICATIONS
AGENCY
ATTN DRCPM-SC
FT MONMOUTH, NJ 07703

DIRECTOR
TRI/TAC
ATTN TT-E-SS, CHARNICK
FT MONMOUTH, NJ 07703

COMMANDER-IN-CHIEF
ATLANTIC
ATTN J6
NORFOLK, VA 23511

COMMANDER
NAVAL ELECTRONIC SYSTEMS COMMAND
ATTN PME 110-241D, D. O'BRYHIM, A. LARSON
WASHINGTON, DC 20360

CHIEF OF NAVAL MATERIEL
THEATER NUCLEAR WARFARE PROJECT OFFICE
ATTN PM-23, TN-31, TATE
WASHINGTON, DC 20360

COMMANDER
NAVAL OCEAN SYSTEMS CENTER
ATTN CODE 7309, R. GREENWELL
ATTN CODE 8123, S. LICHTMAN
ATTN CODE 83, J. STAWISKI
SAN DIEGO, CA 92152

COMMANDING OFFICER
NAVAL ORDNANCE STATION
ATTN STANDARDIZATION DIVISION
INDIAN HEAD, MD 20640

COMMANDER-IN-CHIEF
PACIFIC
ATTN C3S-RP-1
CAMP H. M. SMITH, HI 96861

COMMANDING OFFICER
NAVAL RESEARCH LABORATORY
ATTN CODE 4720, J. DAVIS
WASHINGTON, DC 20375

COMMANDER
NAVAL SURFACE WEAPONS CENTER
ATTN CODE F-56
DAHLGREN, VA 22448

COMMANDER
NAVAL SURFACE WEAPONS CENTER
ATTN CODE F32, E. RATHBURN
ATTN CODE F30
WHITE OAK LABORATORY
SILVER SPRING, MD 20910

DEPARTMENT OF THE NAVY
DIRECTOR, NAVAL TELECOMMUNICATIONS
DIVISION
OFFICE OF THE CHIEF OF NAVAL OPERATIONS
ATTN OP941, HAISLMAIER

DEPARTMENT OF THE NAVY (Cont'd)
ATTN OP943
WASHINGTON, DC 20350

HQ, USAF/SAMI
WASHINGTON, DC 20330

AIR FORCE COMMUNICATIONS COMMAND
ATTN EPPD
SCOTT AFB, IL 62225

COMMANDER US AIR FORCE SPACE COMMAND
ATTN KKO
ATTN KRQ
ATTN XPOW
PETERSON AFB, CO 80912

1842 EEG
ATTN EEISG
SCOTT AFB, IL 62225

HEADQUARTERS
ELECTRONIC SYSTEMS DIVISION/YS
ATTN YSEA
HANSCOM AFB, MA 01730

HEADQUARTERS
USAFE
ATTN DCKI
RAMSTEIN AFB, GERMANY

SYSTEM INTEGRATION OFFICE
ATTN SYE
PETERSON AFB, CO 80912

AIR FORCE WEAPONS LABORATORY/DYC
ATTN NTC4, TESD, IESM
KIRTLAND AFB, NM 87117

CENTRAL INTELLIGENCE AGENCY
ATTN OWSR/NED
ATTN OWSR/STD/MTB, A. PADGETT
WASHINGTON, DC 20505

DIRECTOR
FEDERAL EMERGENCY MANAGEMENT AGENCY
OFFICE OF RESEARCH/NPP
ATTN STATE & LOCAL PROG SUPPORT
500 C STREET, SW
WASHINGTON, DC 20472

FEDERAL PREPAREDNESS AGENCY
GENERAL SERVICES ADMINISTRATION
ATTN ESTE-M MURTHA
18TH & F STREETS, NW
WASHINGTON, DC 20405

LAWRENCE LIVERMORE NATIONAL LAB
ATTN TECHNICAL INFO DEPT LIBRARY
ATTN L-156, H. CABAYAN, L. MARTIN
PO BOX 808
LIVERMORE, CA 94550

DIRECTOR
NATIONAL SECURITY AGENCY
ATTN R15
9800 SAVAGE ROAD
FT MEADE, MD 20755

AMERICAN TELEPHONE & TELEGRAPH CO
ATTN SEC OFC FOR W. EDWARDS
1120 20TH STREET, NW
WASHINGTON, DC 20036

AT&T BELL LABORATORIES
ATTN R. STEVENSON
ATTN J. MAY (3 COPIES)
1600 OSGOOD ST
N. ANDOVER, MA 01845

AT&T BELL LABORATORIES
ATTN J. SCHOLL (5 COPIES)
ATTN J. SERRI
CRAWFORDS CORNER ROAD
HOLMDEL, NJ 07733

BDM CORP
ATTN CORPORATE LIBRARY
7915 JONES BRANCH DRIVE
MCLEAN, VA 22102

BOEING CO
ATTN R. SHEPPE
PO BOX 3707
SEATTLE, WA 98124

COMPUTER SCIENCES CORPORATION
SYSTEMS DIVISION
ATTN A. SCHIFF
1400 SAN MATEO BOULEVARD, SE
ALBUQUERQUE, NM 87108

ELECTROMAGNETIC APPLICATIONS, INC
ATTN R. PERALA
PO BOX 26263
1978 SOUTH GARRISON ST
DENVER, CO 80226

ENGINEERING SOCIETIES LIBRARY
ATTN ACQUISITIONS DEPT
345 EAST 47TH STREET
NEW YORK, NY 10017

GEORGIA INSTITUTE OF TECHNOLOGY
OFFICE OF CONTRACT ADMINISTRATION
ATTN RES & SEC COORD FOR H. DENNY
ATLANTA, GA 30332

IIT RESEARCH INSTITUTE
ATTN J. BRIDGES
ATTN I. MINDEL
10 W. 35TH STREET
CHICAGO, ILL 60616

INTERNATIONAL TEL & TELEGRAPH CORP
ATTN A. RICHARDSON
ATTN TECHNICAL LIBRARY
500 WASHINGTON AVENUE
NUTLEY, NJ 07110

MISSION RESEARCH CORP
PO BOX 7816
ATTN W. STARK
COLORADO SPRINGS, CO 80933

MISSION RESEARCH CORP
EM SYSTEM APPLICATIONS DIVISION
ATTN A. CHODOROW
1720 RANDOLF ROAD, SE
ALBUQUERQUE, NM 87106

PRI, INC
ATTN W. HAAS
6121 LINCOLNIA RD
ALEXANDRIA, VA 22312

RICHARD L. MONROE ASSOCIATES
1911 R STREET, NW
SUITE 203
WASHINGTON, DC 20009

R&D ASSOCIATES
PO BOX 9695
ATTN W. GRAHAM
MARINA DEL REY, CA 90291

R&D ASSOCIATES
ATTN DIRECTOR, DR. J. THOMPSON
1401 WILSON BLVD
SUITE 500
ARLINGTON, VA 22209

ROCKWELL INTERNATIONAL CORP
PO BOX 3105
ATTN D/243-068, 031-CA31
ATTN G. E. MORGAN
ANAHEIM, CA 92803

SCIENCE APPLICATIONS, INC
PO BOX 1303
ATTN W. CHADSEY
McLEAN, VA 22102

SCIENCE ENGINEERING ASSOC
ATTN P. FLEMMING
ATTN V. JONES
MARINER SQUARE
SUITE 127

SCIENCE ENGINEERING ASSOC (Cont'd)
1900 N. NORTHLAICE WAY
PO BOX 31819
SEATTLE, WA 98103

SRI INTERNATIONAL
ATTN A. WHITSON
ATTN E. VANCE
333 RAVENSWOOD AVENUE
MENLO PARK, CA 94025

TRW DEFENSE & SPACE SYSTEMS GROUP
ATTN J. PENAR
ATTN W. GARGARO
ONE SPACE PARK
REDONDO BEACH, CA 92078

TRW DEFENSE & SPACE SYSTEMS GROUP
ATTN E. P. CHIVINGTON
2240 ALAMO, SE
SUITE 200
ALBUQUERQUE, NM 87106

TRW, INC
COMMAND & CONTROL & COMMUNICATIONS
SYSTEM DIV
ATTN N. STAMMER
5203 LEESBURG PIKE
SUITE 310
FALLS CHURCH, VA 22041

US ARMY ELECTRONICS RESEARCH &
DEVELOPMENT COMMAND
ATTN COMMANDER, DRDEL-CG
ATTN TECHNICAL DIRECTOR, DRDEL-CT
ATTN PUBLIC AFFAIRS OFFICE, DRDEL-IN

COMMANDER
HARRY DIAMOND LABORATORIES
ATTN D/TSO/DIVISION DIRECTORS
ATTN RECORD COPY, 81200
ATTN HDL LIBRARY, 81100 (3 COPIES)
ATTN HDL LIBRARY (WOODBRIDGE)
ATTN TECHNICAL REPORTS BRANCH, 81300
ATTN LEGAL OFFICE, 97000
ATTN CHIEF, 21000
ATTN CHIEF, 21100
ATTN CHIEF, 21200
ATTN CHIEF, 21300
ATTN CHIEF, 21400
ATTN CHIEF, 21500
ATTN CHIEF, 22000
ATTN CHIEF, 22100
ATTN CHIEF, 22300
ATTN CHIEF, 22800
ATTN CHIEF, 22900
ATTN CHIEF, 20240
ATTN R. MANRIQUEZ, 21300 (50 COPIES)
ATTN R. REYZER, 21300
ATTN J. SWETON, 21300

END

FILME

11-84

DTIC